Sub – 15 Femtosecond Pulse Generation From a Kerr – Lens Mode – Locked Cr:LiSAF Laser Near 850 nm with a Gain – Matched Output Coupler

by

Ferda CANBAZ

A Thesis Submitted to the

Graduate School of Engineering

in Partial Fulfillment of the Requirements for

the Degree of

Master of Science

in

Optoelectronics and Photonics Engineering

Koç University

September 2013

Koç University

Graduate School of Sciences and Engineering

This is to certify that I have examined this copy of a master's thesis by

Ferda CANBAZ

and have found that it is complete and satisfactory in all respects,

and that any and all revisions required by the final

examining committee have been made.

Committee Members:

_____

Alphan Sennaroğlu, Ph. D. (Advisor)

_____

Ümit Demirbaş, Ph. D.

_____

Alper Kiraz, Ph. D.

Date: _____

ABSTRACT

Generation of ultrashort laser pulses with long–term stability and robustness is very important for many applications such as material processing, biomedical imaging, and spectroscopy. Kerr–lens mode–locking (KLM) is one of the well–known techniques used to generate ultrashort pulses. One drawback of the KLM method is that the modulation depth resulting from the Kerr nonlinearities is typically weak especially in lasers with low nonlinear refractive index. This makes it very difficult to apply the KLM technique to colquiriite type gain media such as Cr:LiCAF and Cr:LiSAF which have low nonlinear refractive indices. Recently, a novel approach has been proposed to overcome this drawback by using what can be referred to as gain–matched output couplers (GMOC). The spectral transmission characteristics of a GMOC are designed in such a way as to provide a higher effective gain for a broadband pulse as opposed to a continuous wave beam, which favors the mode–locked operation of a laser oscillator with much higher temporal stability. In this thesis work, this approach which utilizes the GMOC technology has been applied to a low–cost, directly diode pumped Cr:LiSAF laser around 850 nm. In the experiments, we used a low–cost red diode around 660 nm which could pump the Cr:LiSAF laser without any cooling requirement. An astigmatically compensated x–fold cavity was constructed to house a 6 mm long, 1.5 % Cr doped LiSAF crystal. The GMOC mirror used in the experiments had a transmission of 0.7 % near the center wavelength of the emission band. To obtain the shortest pulses, dispersion compensation was used with chirped mirrors and fused silica prism pairs. In this case, the net cavity dispersion was around ~–50fs^2. When KLM operation was initiated with the GMOC mirror, this configuration resulted in the generation of nearly transform–limited pulses as short as 13 fs, with 25 mW of average output power, at a repetition rate of 126 MHz near 855 nm. Other cases with different levels of cavity dispersion and the tunability of the femtosecond laser were also

investigated. The experimental results clearly demonstrated that the use of a GMOC mirror enables a very robust and stable operation of a Cr:LiSAF laser despite the fact that the nonlinear refractive index of the medium is low.

ÖZET

Kararlı ultra kısa süreli darbe üretebilen ve uzun süre çalışabilen lazerler, malzeme işleme, biyomedikal görüntüleme ve spektroskopi alanlarında birçok uygulamaya sahiptir. Ultra kısa darbe üretiminde Kerr–odaklamalı kip–kilitleme (KLM) yöntemi en çok kullanılan ve en bilinen tekniklerdendir. KLM yöntemindeki en önemli dezavantajlardan biri, doğrusal olmayan kırılma indisinin küçük olduğu malzemelerde, Kerr etkisinin de zayıf olarak gözlenmesidir. Bu da modülasyon derinliğini azaltmakta ve dolayısıyla, kararlı bir şekilde kip kilitli rejimde çalışmayı zorlaştırmaktadır. Bundan dolayı, Cr:LiCAF ve Cr:LiSAF gibi düşük doğrusal olmayan kırılma indisine sahip olan kazanç ortamları ile KLM elde etmek oldukça zordur. Doğrusal olmayan kırılma indisinden kaynaklanan bu zorluğu aşmak için son yıllarda, özgün bir yöntem olan kazanç eşleşmeli çıkış aynası (GMOC) kullanımı önerilmiştir. GMOC aynasının geçirgenlik spektrumu kip–kilitli rejiminde, sürekli dalga rejimine göre daha yüksek optik kazanç sağlayacak şekilde tasarlanmıştır. Bu da lazerin zamanda kararlılığını artırmaktadır. Bu çalışmada, bu yaklaşımla GMOC teknolojisi 850 nm civarında çalışan düşük maliyetli diyot ile direk pompalanan bir Cr:LiSAF lazerine uygulanmıştır. Deneylerde, ekonomik, 660 nm civarında çalışan bir diyot lazeri, herhangi bir soğutma sistemine ihtiyaç duyulmadan pompa olarak kullanılmıştır. Astigmatik sapması düzeltilmiş, x rezonatörü içerisine 6 mm uzunluğunda ve % 1.5 Cr katkılanmış LiSAF kristali yerleştirilmiştir. Deneylerde kullanılan GMOC aynasının merkez dalga boyu civarındaki geçirgenliği % 0.7'dir. En kısa süreli darbeleri elde edebilmek için, lazer rezonatörü içerisine eksi dispersiyona sahip aynalar ve prizma çifti yerleştirilmiştir. Bu durumda net rezonatör dispersiyonu –50 fs^2 civarındadır. GMOC aynası yardımıyla KLM rejimi başlatıldığında, bu tasarımda 13 fs uzunluğunda, 25 mW ortalama güce sahip, merkez dalgaboyu 855 nm'de ve tekrarlama frekansı 126 MHz olan darbeler üretilmiştir. Ayrıca, farklı dispersiyon değerlerinde kip–kilitli rejimin çalışma özellikleri incelenmiş ve femtosaniye lazerin çıkış dalgaboyu 850 civarında ayarlanabilmiştir. Deneysel sonuçlar,

GMOC aynası kullanılarak, doğrusal olmayan kırılma indisi küçük Cr:LiSAF lazeri ile kararlı ve dayanaklı bir şekilde femtosaniye darbe üretilebileceğini göstermiştir.

ACKNOWLEDGMENTS

During this thesis work, lots of people motivated me and supported me. This part of the thesis is dedicated to them. First, I would like to thank my advisor Alphan Sennaroğlu because of his endless patience and dedication to teach. I feel really lucky since he gave me the opportunity to work in the Koç University Laser Research Laboratory (LRL) under his supervision. In the research process, he always keeps me motivated about whatever I work on. In addition, I look forward to working with him and the LRL members in the next four years.

I was also very lucky to have interacted with Adnan Kurt. He always fed me with numerous laboratory skills and original ideas. Working with him is really exciting. I am very delighted to have his support.

I would like to thank Ümit Demirbaş for his support and friendly collaboration during my thesis work. I was really inspired by his way of thinking and passion forwork.

I am very grateful about the friendly environment of our laboratory. I especially want to thank M. Natali Çizmeciyan because of her support in developing my experimental skills. Another member of the LRL group that I greatly appreciated is Ersen Beyatlı. He always helped me and I believe that he will always continue to help. I would like to thank Işınsu Baylam because of her straightness and friendship. I also would like to thank the other members of our laboratory, Can Cihan, İsmail Yorulmaz, Philipp Heck, Cem Yetişmişoğlu and Merve Şahin because of their friendship and support.

Alper Kiraz deserve special thanks as my thesis committee members. I also would like to thank Sarper Özharar because of his valuable ideas and friendship.

I am very thankful to have such open-minded parents as Halil İbrahim and Semiha Canbaz. They have been supporting me in each step of my life. My sisters Funda Sevimli

and Fulya Toprak are “the architects of my life”. The last member of our family is Azra Sevimli. She is my little nephew and breath of life.

I am grateful to have a friend as Tuğba Nur Öztürk. She is always the best companion for me. She is also the only person that I can discuss about everything and everyone☺.

I would like to thank Serdar Özege for his love and patience.

Last but not least, I would like to thank my generation to have the power of resistance and the love of nature. I want to dedicate this thesis work to the resisters who have been part of the civilian resistance all over the World.

TABLE OF CONTENTS

LIST OF FIGURES

LIST OF TABLES

NOMENCLATURE

σ_a:	Absorption cross–section	l_G:	Optical path between two gratings
β:	Angle of diffraction	φ_0:	Phase
α:	Angle of incidence	h:	Planck's constant
ω:	Angular frequency	ΔN:	Population inversion
ω_0:	Beam waist spotsize	P:	Power
λ_0:	Central wavelength	W:	Pulse energy
β:	Chirp parameter	τ_{Pulse}:	Pulsewidth
l_C:	Crystal length	I_P:	Pump intensity
A_{eff}:	Effective area	z_0:	Rayleigh range
E:	Electric field amplitude	f_{rep}:	Repetition rate
σ_e:	Emission cross–section	L_R:	Resonator length
N_2:	Excited state population density	T_R:	Roundtrip time
v_P:	Frequency of pump photons	E_{sat}:	Saturation energy
v_L:	Frequency of laser photons	l_P:	Separation between two prisms
g:	Gain	η:	Slope efficiency
N_1:	Ground state population density	g_0:	Small signal gain
D:	Group delay dispersion (GDD)	c:	Speed of light
δ:	Kerr coefficient	l_S:	Substrate length
ω_L:	Laser beam waist	G_{th}:	Threshold gain
I_L:	Laser intensity	P_{th}:	Threshold power

L:	Loss	T:	Transmission
α_L:	Material loss	λ:	Wavelength
n_2:	Nonlinear refractive index	k:	Wave number
P:	Optical path	$\omega(z)$:	Spotsize function
M^2	Diffraction parameter	z_0:	Rayleigh range
α_T:	Cavity total losses	R_1,R_2:	End mirrors reflectivities
τ_f:	Fluorescence lifetime	T_R:	Cavity round trip time
τ_P:	Cavity photon lifetime	E_{sat}:	Saturation energy
d:	Effective length of the resonator		

1 INTRODUCTION

1.1 Motivation

This thesis is concerned with the development of a new class of stable and robust femtosecond laser systems based on a new mirror design known as the gain matched output coupler. In a femtosecond laser, a tunable gain medium is used to provide laser emission over a broad wavelength range. To obtain short pulses, the longitudinal modes supported by the resonator are locked to oscillate with a nearly constant phase, resulting in the generation of a periodic train of pulses which are much shorter than the round trip time of the resonator. With typical tunable gain media with spectral bandwidths of several THz, pulses with duration in the femtosecond range can be obtained. Femtosecond sources are useful in many applications such as micromachining [1], spectroscopy [2-4], and biomedical imaging [5, 6], in which especially lasers around ~800 nm are very commonly used.

Many different techniques can be used to obtain mode–locked operation from a laser. One of these is the well–known Kerr–lens mode locking (KLM) technique which has been applied to many solid state lasers to generate femtosecond pulses. Here, the mode–locked operation is initiated by fine adjustment of lensing in the gain medium which has Kerr–nonlinearity. In this case, a higher intensity laser beam sees a stronger lensing and has a better overlap with the pump beam. This gives a higher optical gain in comparison with what is experienced by a low intensity beam. Hence, Kerr lensing favors the oscillation of a high intensity beam and triggers the laser to operate in a mode–locked regime and produce femtosecond pulses. In gain media with low nonlinear refractive index, it becomes difficult to operate the laser in Kerr lens mode–locked regime and the laser often becomes unstable. It is therefore important to develop techniques which can improve the operational stability of a KLM femtosecond laser even when the gain medium has a low nonlinear refractive index. The approach used in this thesis employs a special kind of a mirror, known as a gain matched

output coupler (GMOC), to achieve a higher stability during KLM operation in media with low Kerr nonlinearities.

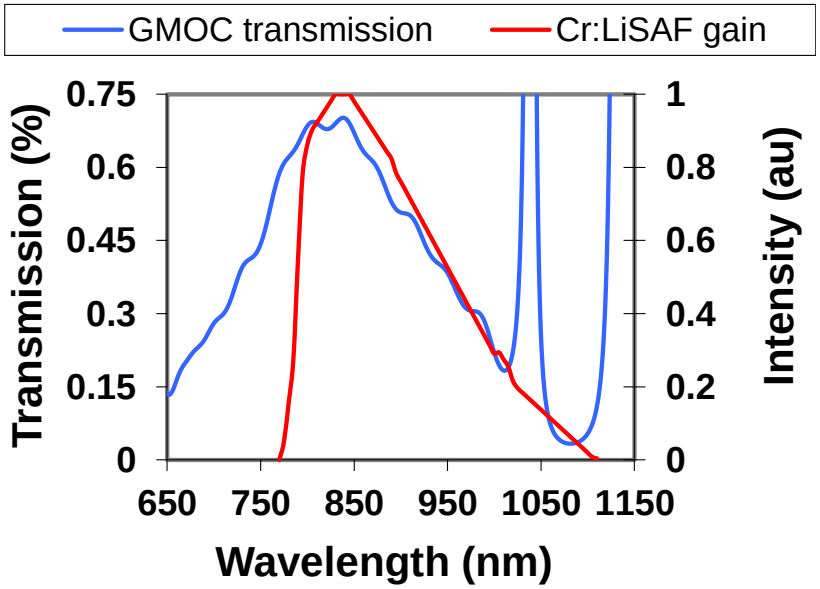

Figure 1. 1: Transmission spectra of GMOC and emission spectra of Cr:LiSAF

The transmission spectrum of a GMOC mirror matches the emission spectrum of the gain medium as shown in Fig. 1.1. As can be seen here, when the transmission spectrum matches the emission profile, a broadband pulse circulating in the resonator sees an effectively higher optical gain per round trip, in comparison with a continuous wave signal which has a narrow bandwidth. Hence, the effective modulation depth of mode locking can be considerably enhanced with a GMOC mirror. As a consequence, even when the nonlinear refractive index of the gain medium is low, stable and robust KLM operation can be achieved.

In this thesis work, we applied this technique to stabilize the operation of a 850 nm Cr:LiSAF laser which has a significantly lower nonlinear refractive index as compared with Ti:Sapphire. With use of a GMOC mirror, pulses as short as 13 fs were generated from the Cr:LiSAF laser with long–term operational stability. A major reason for applying this technique to Cr:LiSAF laser is that, it has the potential to replace the currently used Ti:Sapphire lasers in the same wavelength range which are far more expensive to build. This is because Cr:LiSAF can be directly diode pumped with low cost diodes operating in the red wavelength range whereas currently used Ti:Sapphire lasers need much more expensive green pump sources.

The Cr:LiSAF gain medium belongs to the family of solid state laser crystals known as Cr:Colquiriites. In the following sections of this chapter, we first provide a general overview of the Cr:Colquiriite gain media and discuss their optical as well as thermal properties. In particular, we introduce the important material parameters such as stimulated emission cross section, nonlinear refractive index, fluorescence lifetime and thermal conductivity. We then compare the quantum electronic properties of Colquiriites with those of Ti:Sapphire lasers and explain why it is possible to directly diode pump the Cr:colquiriites. A brief discussion about the mode locking techniques is also provided. Finally, we discuss in more detail why the GMOC mirror provides a more effective modulation depth during KLM operation.

1.2 General Overview of Cr:Colquiriite and Ti:Sapphire Lasers

Especially lasers around ~800 nm are commonly used in many applications such as micromachining [1], spectroscopy [2-4], and biomedical imaging [5, 6]. In the visible and the near infrared range, Ti:Sapphire ($Ti:Al_2O_3$) and Cr–doped colquiriite lasers as well as their second or third harmonic outputs are widely utilized owing to their broadband wavelength tunability. Among tunable solid state lasers, Ti:Sapphire has the broadest tuning range from 660 to 1180 nm and the ability to directly generate as short as 5–fs pulses [7-10]. Theoretically, the shortest pulses that can be generated from Ti:Sapphire lasers have a duration of 3.6–fs [11]. One drawback, however, is that generally, Ti:Sapphire lasers are pumped by frequency doubled neodymium lasers which are bulky and costly. As a solution, Cr:Colquiriite lasers can be used instead of the Ti:Sapphire lasers to lower the overall system cost. This is because, Cr doped colquiriites have absorption bands around 660 nm and can be directly diode pumped with commercially available single–mode low–cost red diodes [12]. In addition, the emission bands of the Cr–doped colquiriites [13-15] and Ti:Sapphire have a very good overlap as can be seen from Fig. 1.1.

Before providing further discussion about the Cr:colquiriite gain media, we briefly overview the optical properties of the Ti:Sapphire gain medium as well. As mentioned before, Ti:Sapphire has the broadest tunability range among all known solid–state lasers, capable of supporting ultrashort optical pulses. Kerr–lens mode locking (KLM) is one of the mode locking techniques that depends on the nonlinear refractive index (n_2) of the medium used to achieve ultrashort pulses. The nonlinear refractive index (n_2) is an intensity dependent

refractive index parameter of the medium and n_2 of Ti:Sapphire is 3.2×10^{-16} cm^2/W [16] which is a relatively large value. Nonlinear phase distortions originating from the Kerr effect need to be balanced with a reasonable amount of negative dispersion to obtain stable solitary pulses. In addition, the fluorescence lifetime, emission cross section and the cross–section–lifetime product for Ti:Sapphire crystal are 3.2 μs, 41×10^{-20} cm^2, and $\sigma_e\tau = 131$ μs cm^2, respectively [17]. The value of the product of the emission cross section and the lifetime of Ti:Sapphire shows that it has the potential to be operated with a low lasing threshold. Far above the lasing threshold, where the laser produces a finite output power, one of the most important factors which affect the thermal stability of the laser is the thermal conductivity of the medium. The thermal conductivity of Ti:Sapphire is 28 W/K.m. Together with diamond, this is one of the highest thermal conductivities among solid–state hosts, making Ti:Sapphire suitable for many scientific and technological applications [18, 19].

In the discussion of the Cr–doped colquiriites, their crystal and laser properties will be introduced first. Then, the thermal and optical properties of colquiriites and Ti:Sapphire will be compared. Colquiriite is the general name of crystal hosts such as LiSAF ($LiSrAlF_6$), LiCAF ($LiCaAlF_6$), and LiSGaF ($LiSrGaF_6$). One of the characteristics of colquiriites is the variation of the crystal refractive index along different crystal directions as in Ti:Sapphire. The absorption and emission spectra of these birefringent hosts can be seen from Fig. 1.2 for two different crystal directions. The difference between the emission spectra of crystal directions and hosts can be clearly visualized. Because of the difference of the emission spectra for individual host materials, the tuning range during laser becomes different: 782–1042 nm, 777–977 nm, and 754–871 nm for LiSAF, LiCAF, and LiSGaF, respectively [12]. Hence, up to now, the shortest pulses that can be generated from colquiriite lasers are 10 (Cr:LiSAF) [20], 9 (Cr:LiCAF) [21], and 14 (Cr:LiSGaF) [22] fs. One important handicap about the generation of much shorter pulses from colquiriite lasers by using KLM is the low nonlinear refractive index values. As stated before, in the case of KLM operation, the cavity dispersion must be balanced with reasonable dispersive optics to obtain solitary pulses. The low n_2 values (0.8 (Cr:LiSAF) [18], 0.4 (Cr:LiCAF) [18], 1.2 (Cr:LiSGaF) [16] $\times 10^{-16}$ cm^2/W) causes a disadvantage since a low amount of dispersion must be introduced to achieve solitary pulses. In that case, because the group delay dispersion of a dispersive mirror always oscillates as a function of wavelength, in practice, it becomes very hard to produce a flat and broadband dispersion curve at a low negative value. Fluctuations in the group delay

dispersion would cause the total cavity dispersion to vary from positive to negative values even over a small wavelength range and prevent the initiation of stable solitary pulses.

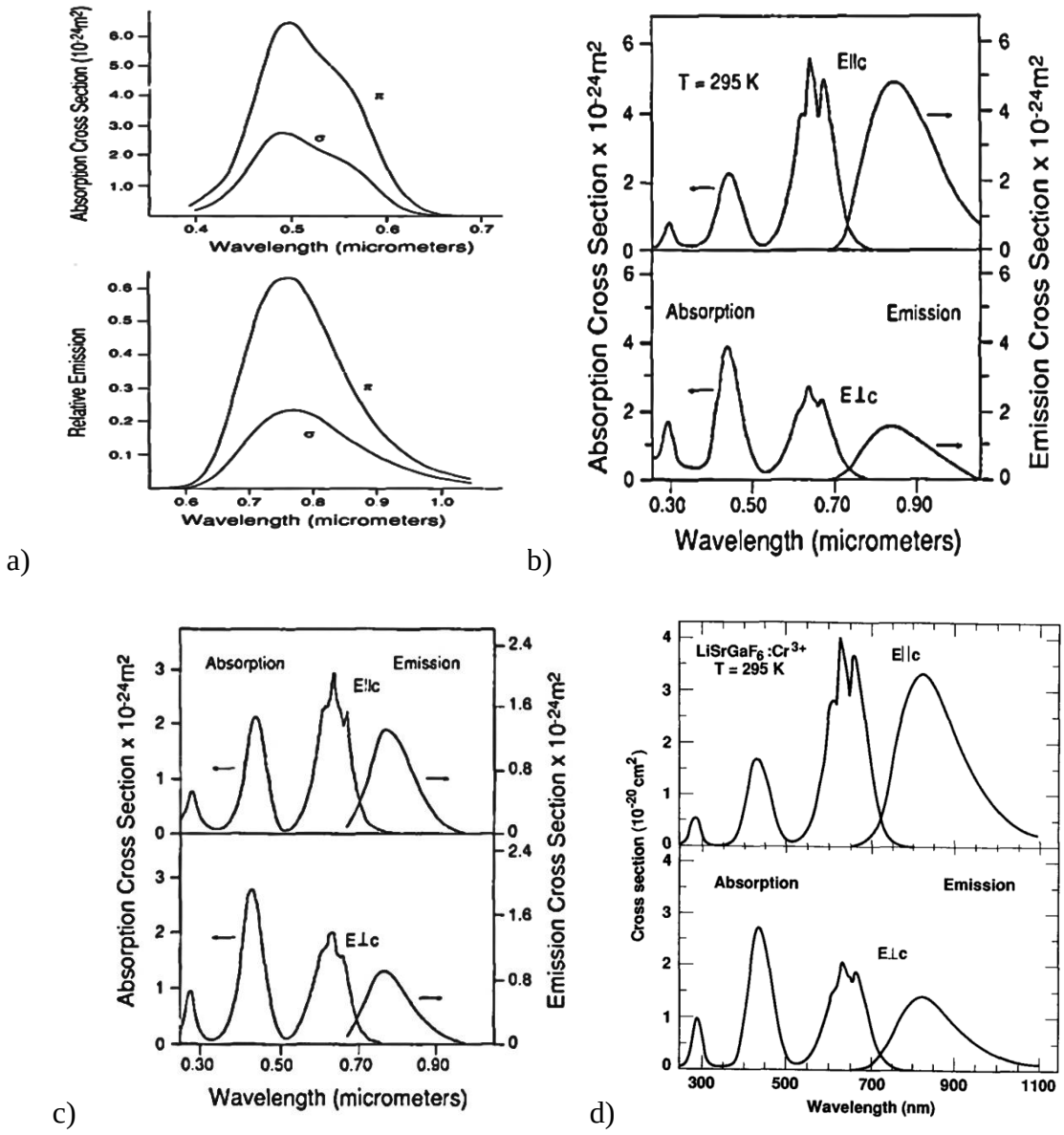

Figure 1.2: Absorption and emission spectrum of a) Ti:Sapphire b) Cr:LiSAF (Adopted from Ref [14]) c) Cr:LiCAF (Adopted from Ref [13]), and d) Cr:LiSGaF (Adopted from Ref [15])

Another important advantage of colquiriites is that Cr:Colquiriite lasers can be directly pumped by low–cost diodes whereas Ti:Sapphire lasers are currently pumped by costly frequency doubled Nd based lasers. Although a lot of progress has been made with green diode pumped Ti:Sapphire systems, there remains room for improvement. Additionally, the product of the peak emission cross section and lifetime ($\sigma_e\tau$) of Cr–doped colquiriites (322, 228, and 290 $\mu s \times 10^{-20} cm^2$ for Cr:LiSAF, Cr:LiCAF, and Cr:LiSGaF, respectively) are two

times larger than that for Ti:Sapphire [17]. As stated before, that larger the emission cross section–lifetime product, the lower is the pump threshold for laser operation. On the other hand, to obtain a thermally stable laser operation, the thermal conductivity value is also significant. Compared to Ti:Sapphire, the thermal conductivities of colquiriites are much lower (Cr:LiSAF : 3.1, Cr:LiCAF : 5.1 [18], Cr:LiSGaF : 3.6 [16] W/K.m). This could pose a serious problem during high power operation. However, the thermal conductivities are sufficient to operate these lasers at room temperature without any cooling mechanism when they are pumped by low–power single mode diodes with few hundreds of mWs of output power.

In addition to Kerr lens mode locking, another method to obtain mode–locking from a laser cavity is by using saturable absorbers such as semiconductor saturable absorber mirrors (SESAMs, which are also known as saturable Bragg reflectors or SBRs) or nanostructured carbon based saturable absorbers (SAs) (single wall carbon nanotubes (SWCNTs), and graphene based saturable absorbers). The most important disadvantage of using SESAMs or SBRs in the case of ultrashort pulse generation is that, unlike KLM, because of the design of the mirrors, bandwidth limitation shows up [23, 24]. In the saturable absorber case, to saturate the absorber, one needs to build another beam waist cavity inside the resonator. One drawback is that, even if the additional mirrors are highly reflective, they introduce additional losses into the cavity and raise the threshold pump power needed to obtain lasing. In contrast, KLM does not need any additional system, thus the only limitation will be the gain bandwidth of the gain medium and the control of dispersion to achieve a constant phase across the full bandwidth. Since its invention in the early 1990s[11], mode–locking via Kerr nonlinearities has become a widely used method to generate ultrashort pulses and has been successfully demonstrated in many gain media such Ti Sapphire [11], Cr:Forsterite [25], Cr:ZnSe [26], Cr:YAG [27], Cr:LiCAF [28], Cr:LiSGaF [29], and Cr:LiSAF [30].

This thesis mainly focuses on Cr:LiSAF systems, and to provide a brief historical review, some of the earlier work on Cr:LiSAF lasers will now be discussed. The Cr:LiSAF laser was first demonstrated by Payne *et al.* in 1989 [14]. Since then, it has always been an attractive material, considering its broadband gain bandwidth and high gain among Cr:Colquiriites. In recent years, Cr:Colquiriites became attractive once again with the invention and widespread use of low–cost diodes (around 660nm). The absorption bands of colquiriites are near the red region in the electromagnetic spectrum. In the very first years

after their invention, the output power level of the diodes was really low. However, since the passive losses of Cr:LiSAF are low and the the product of the emission cross section and lifetime ($\sigma_e\tau = 322$ μs cm^2) is large [17], it is possible to achieve laser operation at low pump powers. In 1991, Scheps *et al.* demonstrated the first diode pumped Cr:LiSAF system [31]. After a short time, the first diode–pumped cw–mode–locked Cr:LiSAF laser was reported by Valentine *et al.* in 1999 [32]. Theoretically, the shortest transform–limited pulse that can be generated from a Cr:LiSAF system is 7.6 fs [30]. Up to now, the shortest pulse that has been directly obtained from a Cr:LiSAF laser was 10 fs [20].

Direct diode pumping provides significant advantages; lower cost, high electrical–to–optical conversion efficiency, compactness, lower noise, and reduced cooling requirements [17, 33-36]. In our system, our motivation is to get a compact, cost–effective, robust, and the shortest pulse output via KLM operation from the Cr:LiSAF gain medium. The nonlinear refractive index of the gain material is very important in order to obtain stable KLM operation. As mentioned before, since the nonlinear refractive index of Cr:LiSAF is low, it is hard to obtain robust and stable Kerr–lens mode–locking. Another important factor is that, KLM operation is typically initiated near the edge of the stability range where poorer mode matching between the pump and the laser beams leads to low output beam quality and low output power. To overcome the limitations arising from the KLM technique, the gain–matched output coupler (GMOC) was introduced by Chen et al. [37, 38] and was first demonstrated in a Ti:Sapphire laser.

To present further information about the working principle of a GMOC mirror, a simplified discussion will be given. The transmission spectrum of the GMOC is designed in such a way as to match the emission spectrum of the gain medium. Hence, this design effectively provides a flat gain profile. In other words, the transmission profile of the GMOC introduces a loss profile which matches with the gain profile of the medium. The perfect match of the two spectra was earlier shown in Fig. 1.1. The flat gain profile causes a higher positive feedback for mode–locking than for continuous–wave operation. Additionally, as a result of these advantages there is no need to operate the laser near the edge of the stability region as in the case of the standard KLM operation. Hence, the output beam quality and the average power are preserved when a GMOC is used.

To provide an introductory discussion about the configuration of our cavity design, dispersion optimization techniques will be introduced briefly. To achieve the shortest pulses

in a cavity, a nearly flat dispersion profile is needed with a low amount of dispersion oscillations. In our system we used both commercially available double–chirped mirrors (DCMs) and a pair of fused silica prisms to obtain an almost flat dispersion profile. Both configurations and results will be discussed in Chapter 3. Before the experimental details and results, a concise overview will be provided about the physical characteristics of optical processes and theory of laser operation in Chapter 2.

2 OPTICAL PROCESSES AND THEORY OF LASER OPERATION

In this chapter, to understand the underlying mechanisms of laser operation, the basic concepts of light–matter interaction and laser operation will be discussed. These include absorption and emission processes, properties of laser light, gain mechanism, lasing threshold condition, and continuous wave and mode–locked analysis of a laser. Finally, the group delay dispersion parameter will be discussed to understand how ultrashort pulses can be generated.

2.1 Optical Processes

The physical mechanism behind laser operation is quite complicated. To provide a simplified, intuitive picture about the operational mechanisms an elementary description will be given in this chapter. In the simplified version, to introduce a laser cavity one needs a pumping light beam, a gain medium, and mirrors which provide positive feedback. Starting with the pump beam; its energy needs to be nearly equal the difference between the energy levels of the gain medium. If they are nearly equal to each other, then the material will absorb the pump light and become excited. After a characteristic time which is of the order of the emission lifetime, the medium gives out its energy via radiative or non–radiative processes. In the radiative case, two different radiation processes occur that are called spontaneous emission and stimulated emission with photon output. If this process is non–radiative, there is no photon output. The output of this process can be in the form of heat. Figure 2.1 provides a simplified sketch to visualize these processes.

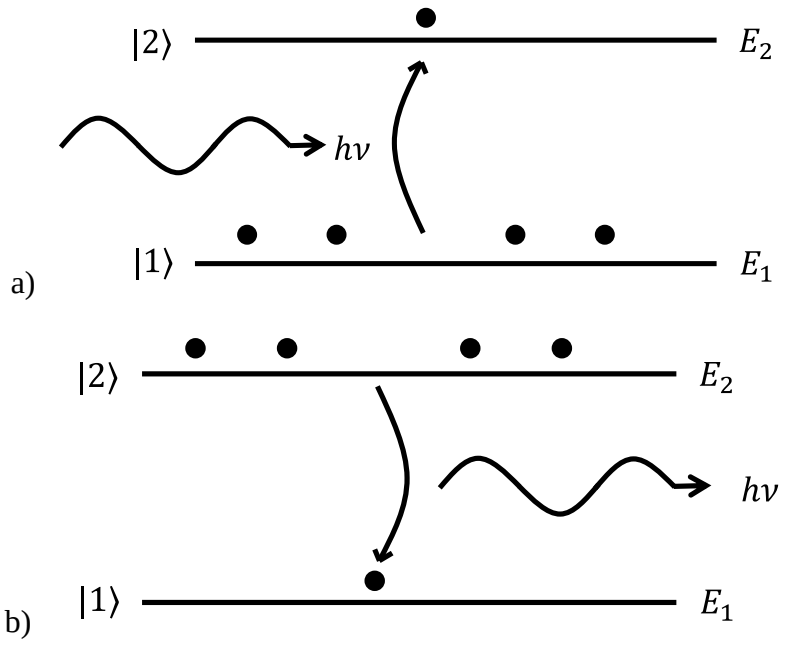

Figure 2.1: a) Absorption and b) Emission processes between two levels of an atomic system (*Adopted from* Ref [39])

In a more detailed description, we first discuss stimulated absorption which is the first case that occurs when light is incident on a material. The incident light which has photon energy approximately equal to the difference between the energy levels of the material, will excite the atoms from the ground state to excited state. This process is called stimulated absorption. In practice, one also needs to account for the fact that the energy levels of an atom are not ideally sharp and the light source may not be monochromatic. To account for the broadening of the atomic levels, we typically introduce the lineshape function (g(ν)). Since there is no monochromatic light in nature, the color distribution function of incoming light is described with the spectral energy density function (ρ(ν)). Stimulated absorption causes an increase in the upper level population, compatible with Einstein's phenomenological model [40]. The absorption process can be modeled with a simple differential equation as

$$\frac{dN_2}{dt} = N_1 B_{12} \int_0^\infty d\nu\, \rho(\nu) g(\nu). \qquad (2.1.2)$$

Here N_1, N_2 are the ion concentrations of level 1 and 2. B_{12} is the Einstein's B coefficient.

Two other processes which occur when light interacts with matter are called spontaneous and stimulated emission. Both are decay processes from the upper to the lower

energy levels. Spontaneous emission occurs, even if there is no pumping mechanism, in random phases, directions and polarization state. It is used to analyze the gain material properties such as the fluorescence lifetime and emission cross section.

Finally, in the stimulated emission process, emitted photons are in the same phase, direction and polarization state as the stimulating light, which is a significant property for building a laser. In a laser, end mirrors are also used to form a cavity which enhances the circulating light as a result of stimulated emission and provides a directional output. A schematic description of stimulated emission can be seen in Fig. 2.2.

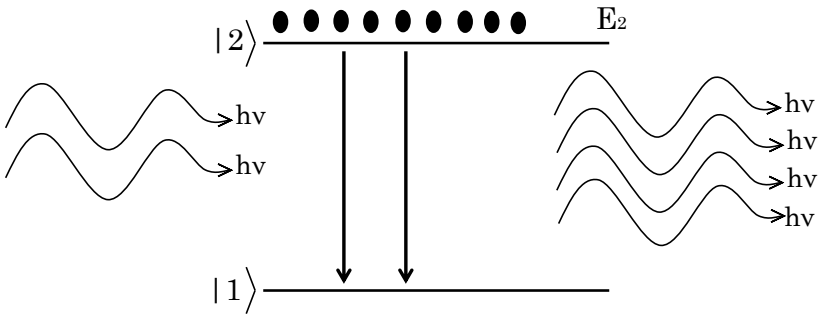

Figure 2.2: Schematic representation of stimulated emission (*Adopted from* Ref [39])

2.2 General Properties of Lasers

2.2.1 Lasers are Oscillators

To provide an intuition about the working principle of lasers, the general properties will be discussed briefly. In a laser, optical gain provided by stimulated emission is combined with the positive feedback provided by the cavity end mirrors to obtain light oscillation at a definite frequency. To clarify the process in the resonator, after the pump beam excites the gain medium, the decaying atoms start to emit light by stimulated emission. If highly reflective mirrors coated at the emission wavelength are placed around the gain medium, light will be continuously reflected. A simple cavity design can be seen from Fig. 2.3. In steady state, the saturated gain equals the passive resonator losses and a finite output power is obtained through one of the partially reflecting end mirrors, known as the output coupler.

Figure 2.3: A sketch of a simple laser cavity

2.2.2 Directionality of Laser Light

As discussed above, once laser oscillation is obtained, the laser output is obtained from one of the partially transmitting end mirrors. Ideally, had there been no diffraction effects, the output beam of the laser would propagate forever without spreading. However, even for the ideal case there are diffraction effects. In the best case, a pure TEM_{00} output can be obtained from a laser cavity, but the propagation distance over which the beam remains close to its initial width is called the Rayleigh range. Due to diffraction, the spotsize function of a cavity can be written as

$$\omega(z) = \omega_0\sqrt{1+\left(\frac{z-z_f}{z_0}\right)^2}, \qquad (2.2.2.1)$$

Where the Rayleigh range can be calculated from

$$z_0 = \frac{n\pi\omega_0^2}{M^2\lambda}. \qquad (2.2.2.2)$$

Above, ω_0 is the beam waist inside the gain medium, z_f is the position of the beam waist, n is refractive index of the gain medium and M^2 gives the diffraction parameter of a beam. M^2 equals 1 for a diffraction limited TEM_{00} output.

2.2.3 Monochromaticity and High Spectral Brightness of Laser Light

The spectral width $\Delta\nu$ of the laser light can be made very small compared to the center frequency ν. Fractional linewidths $(\Delta\nu/\nu)$ as short as 10^{-15} have been achieved [41]. However, the spectral width will never be zero because of natural broadening effect that comes from spontaneous emission. To determine the spectral brightness, power per wavelength needs to be calculated for a source which has an area a and subtend a solid angle of Ω. The relation for calculating the brightness is given by

$$B \equiv \frac{P}{a\Omega\Delta\nu}. \qquad (2.2.3.1)$$

In other words, since the spectral width of the laser output is very small, the brightness will be high.

2.2.4 Coherence of Laser Light

In addition to the other properties of laser light, in this part, coherence of the output beam will be discussed. Qualitatively, the term coherence tells us how close a light source is to an ideal sinusoidal wave. An exact sinusoidal wave at a definite frequency will have perfect coherence, meaning that at any distance from the source, one can produce interference patterns with high contrast. However, realistic beams are usually partially coherent. In this case, there is a characteristic length, known as the coherence length, beyond which it is not possible to obtain an interference pattern. The coherence length is given by

$$l_c = \tau_c . c. \qquad (2.2.4.1)$$

If the wave is also spatially coherent the phase will be fixed on a plane that is perpendicular to the direction of propagation. As a result the cavity will be support only TEM_{00}. A laser beam with a narrow spectral width will tend to have a long coherence length. Typically, the coherence length of a laser is significantly larger than that of an incoherent light source based on spontaneous emission.

2.3 Optical Gain

To generate laser output, the first step involves optical amplification or optical gain inside the laser gain medium. The medium that makes transitions between its energy states by pumping is called a gain medium. If an excited state of the gain medium has higher population than the lower state, this is called population inversion and leads to optical amplification. In other words, when this condition is satisfied, the system provides optical gain. In this thesis, the gain medium is Cr^{3+} doped LiSAF crystal. Since its absorption line is around 660 nm, we are using nearly monochromatic output from a single mode diode as the pumping mechanism. To emphasize the role of optical amplification in our system, a brief derivation of the optical gain equations will be done below for the case of monochromatic excitation. As can be seen from Fig. 2.4, an incoming monochromatic beam excites atoms from the state $|1\rangle$ to state $|2\rangle$ which are occupied by N_1 and N_2 atoms per unit volume, respectively. Assume that the atomic

system has a length of Δz and a cross sectional area of a. The incoming beam has photon energy of

$$h\nu \approx E_2 - E_1 \tag{2.3.1}$$

and is assumed to be a plane wave.

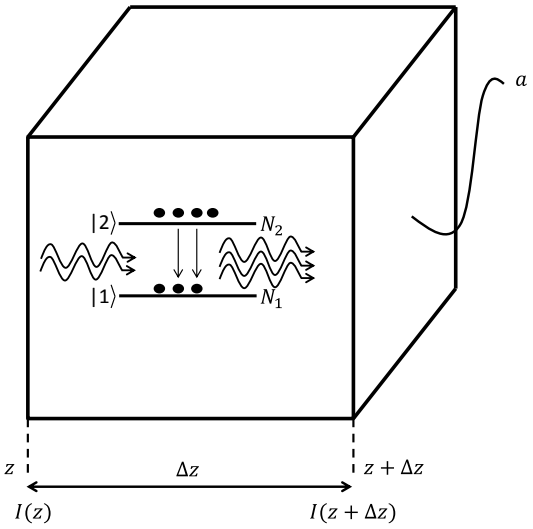

Figure 2.4: Schematic description of a nearly monochromatic light beam through a two level atomic medium which has a length of Δz (*Adopted from* Ref[39])

Stimulated absorption causes a decrease in the intensity of the pump light and hence reduces the number of pump photons. At the same time, stimulated emission adds coherent photons to the signal wave at the laser wavelength. In the analysis of optical amplification, contribution of spontaneous emission is neglected. The rate equation for the upper level population hence becomes

$$\frac{dN_2}{dt} = -B_{21}N_2\rho_\nu g(\nu). \tag{2.3.2}$$

Using the intensity relation and the relation between Einstein's A and B coefficients (see Ref. 39 for a detailed analysis), Eq. 2.3.2 becomes

$$\frac{dN_2}{dt} = -\frac{c^3 n I N_2 A_{21}}{n^3(8\pi h\nu^3)c} g(\nu) = -\frac{A_{21}\lambda^2}{8\pi n^2} g(\nu)\left(\frac{I}{h\nu}\right) N_2. \tag{2.3.3}$$

Therefore, the net rate of change including the contributions of both stimulated absorption and stimulated emission is

$$\frac{dN_2}{dt} = -\sigma_e\left(\frac{I}{h\nu}\right) N_2 + \sigma_a\left(\frac{I}{h\nu}\right) N_1. \tag{2.3.4}$$

Above, σ_e is defined as the stimulated emission cross section which can be alternatively expressed as

$$\sigma_e = \frac{A_{21}\lambda^2}{8\pi n^2} g(\nu). \quad (2.3.5)$$

Similarly, the stimulated absorption cross–section σ_a can be calculated from

$$\sigma_a = \frac{g_2}{g_1}\frac{A_{21}\lambda^2}{8\pi n^2} g(\nu)\ . \quad (2.3.6)$$

The stimulated emission cross section can be defined in words as the ratio of the stimulated decay rate per atom to the stimulating flux and has the unit of area (cm^2). It is an important parameter needed in the calculation of the fractional power gain resulting from stimulated emission.

To determine the increase in the power output, assuming each downward transition adds one photon of energy hν to the propagating beam, the net rate of change will be multiplied by the volume (cross sectional area x dz) and the photon energy. However, since stimulated emission shows a decrease in the upper state population, an increase in the output power must be obtained by the negative of the net rate of change equation.

$P(z)$ and $P(z + dz)$ correspond to the powers at the positions of z and $z + dz$, respectively and are related according to

$$P(z + dz) - P(z) = a\big(I(z + dz) - I(z)\big) \quad (2.3.7)$$

$$-\left(\frac{dN_2}{dt}\right)(a\Delta z h\nu) = \sigma_e \frac{I}{h\nu}(N_2 - \frac{g_2}{g_1}N_1) a h\nu \Delta z. \quad (2.3.8)$$

In the limit of $deltaz \to 0$, the difference equation can be written as a differential equation as follows:

$$\frac{I(z+dz)-I(z)}{dz} = \frac{dI}{dz} = \gamma(\nu) I. \quad (2.3.9)$$

In Eq. (2.3.9), $\gamma(\nu)$ is the differential gain coefficient given by

$$\gamma(\nu) = \sigma_e\left(N_2 - \frac{g_2}{g_1}N_1\right) = \sigma_e \Delta N. \quad (2.3.10)$$

Also, ΔN is the population inversion which can be expressed according to

$$\Delta N = \left(N_2 - \frac{g_2}{g_1}N_1\right). \quad (2.3.11)$$

To achieve optical amplification from a system, we must satisfy the condition $\left(\frac{dI}{dz} > 0\right)$. In other words, the population inversion needs to be positive $(\Delta N > 0)$. To get a higher population at the excited state ($N_2 > N_1$), we need a non–equilibrium state where an external source is used to pump atoms from the ground state to the excited state. Because, according to the well–known Boltzmann statistics, the occupation numbers of energy states decreases exponentially with increasing energy in thermal equilibrium and the amplification condition is never satisfied unless an external energy source is used for pumping atoms to the upper level.

2.4 Threshold Condition and Continuous Wave Analysis of Laser Operation

Before the analysis of continuous–wave laser operation, the threshold condition for laser oscillation is discussed first. Even if the mirrors in the laser resonator are highly reflective, there will be losses originating from the imperfections in the coatings, scattering in the gain medium and also parasitic absorption bands in the gain medium. Hence, the propagating light inside the cavity needs to overcome these losses before laser oscillation can start. In other words, a threshold population inversion, and alternatively, a threshold pumping level needs to be reached before the laser begins to produce a finite output power. In a laser cavity at the threshold pump power, the gain is exactly equal to the losses. When the passive losses of a cavity are taken into account, the intensities of the circulating beam after two consecutive round trips are related through

$$I_{m+1} = I_m R_1 R_2 \exp(-2\alpha_L d_g) = I_m \exp(-2\alpha_T d_g) . \qquad (2.4.1)$$

In Eq. (2.4.1), R_1 and R_2 are the reflectivities of the end mirrors, α_L is the differential passive loss coefficient and d_g is the length of the crystal. Also,

$$\alpha_T = \alpha_L + \frac{1}{d_g} \ln\left(\frac{1}{R_1 R_2}\right), \qquad (2.4.2)$$

where α_T includes all the losses inside the cavity as if all of them were distributed over the crystal.

As is shown in detail in Ref. 39, two coupled differential equations can be derived to describe the time evolution of the power gain G(t) and the intracavity laser power $P_L(t)$ in a laser resonator:

$$\frac{dG}{dt} = -\frac{G(t)-G_0}{\tau_f} - \frac{P_L(t)G(t)}{E_{sat}} \quad (2.4.3)$$

$$\frac{dP_L}{dt} = -\frac{P_L(t)}{\tau_p} + \frac{2G(t)P_L(t)}{T_R}. \quad (2.4.4)$$

In Eq. 2.4.3, the power gain G(t) can be calculated in terms of the emission cross–section, upper–state population density (for a 4–level system) and the length of the gain medium as $G = \sigma_e N_2 d_g$. At the lasing threshold there is no output from the laser. Hence, $P_L = 0$ and $G = G_{th}$. If we start with the continuous wave operation, the time derivatives will be zero and the calculated threshold gain becomes

$$G_{th} = \frac{T_R}{2\tau_p}. \quad (2.4.5)$$

The expression for G_{th} can be used in the steady state analysis. In the case of the steady state analysis, the saturated gain equals the total loss which, in turn, is equal to the threshold value of the power gain. As a result, we have

$$G_s = G_{th} = \frac{G_0}{1+\frac{P_L}{P_{sat}}} = \frac{T_R}{2\tau_p} = \alpha_L + \frac{1}{d_g}\ln\left(\frac{1}{R_1 R_2}\right). \quad (2.4.6)$$

The output power of the laser also depends on the reflectivity of the output coupling mirror and can be calculated by using

$$P_{out} = (1 - R_2)\frac{P_{sat}}{2}\left(\frac{G_0}{G_{th}} - 1\right). \quad (2.4.7)$$

To calculate the threshold pump power, we will assume that $R_1 = 1$ and $R_2 = 1 - T$. R_1 is the reflectivity of the high reflector mirror and R_2 is the reflectivity of the output coupler. During one round trip, light must pass through the gain medium twice in a standing-wave resonator. Therefore, the material loss will be

$$L = 2\alpha_L d_g. \quad (2.4.8)$$

Using Eq. 2.4.4, $G_{th} = \frac{1}{2}[L + T]$ is obtained. In the case of Cr:LiSAF which can be treated as an ideal four level system, the threshold pump power can be obtained from

$$(P_p)_{th} = A(L + T). \quad (2.4.9)$$

A is constant in Eq. 2.4.9. A can be determined experimentally if the threshold pump power is measured for different output coupling levels. The ratio of the intercept to the slope of the threshold power–OC transmission curve gives the round trip loss L

Above the lasing threshold, the laser begins to produce a finite output power. The slope efficiency, which gives the increase in the output power per unit change in the pump power, can be calculated by using the following expressions:

$$\eta = \frac{\Delta P_{out}}{\Delta P_p} = \frac{T\left(\frac{1}{2}\right)\frac{h\nu_L}{\sigma_e \tau_f} a \sigma_a n_g \sigma_e d_g \tau_f}{\frac{1}{2}(L+T) a h \nu_p} = \frac{\lambda_p}{\lambda_L} \frac{T}{T+L} \eta_a \tag{2.4.10}$$

$$\eta_a = \sigma_a N_g d_g \approx \sigma_a N_T d_g. \tag{2.4.11}$$

When all of the pump power is absorbed ($\eta_a \approx 1$) and the passive resonator losses are low, the slope efficiency approaches λ_p/λ_L which is known as the quantum efficiency. With a knowledge of the threshold pump power and the slope efficiency, the output power of a laser can be estimated by using

$$P_{out} = \eta(P_p - (P_p)_{th}). \tag{2.4.12}$$

2.5 Mode–locking Theory

Mode locking is a technique with which one can generate ultrashort pulses from a laser. Typically, an ultrashort pulse refers to a pulse that has duration significantly shorter than the cavity round trip time. Mode–locking is an operation type to attain ultrashort pulse output from a laser cavity. In a standing wave cavity, several axial modes typically oscillate simultaneously. Mode–locking is a mechanism that describes the phase locking of these modes. In Fig 2.5, the modes that are oscillating inside a cavity can be seen for two cases: 1) oscillation with random phases and 2) oscillation with a constant phase.

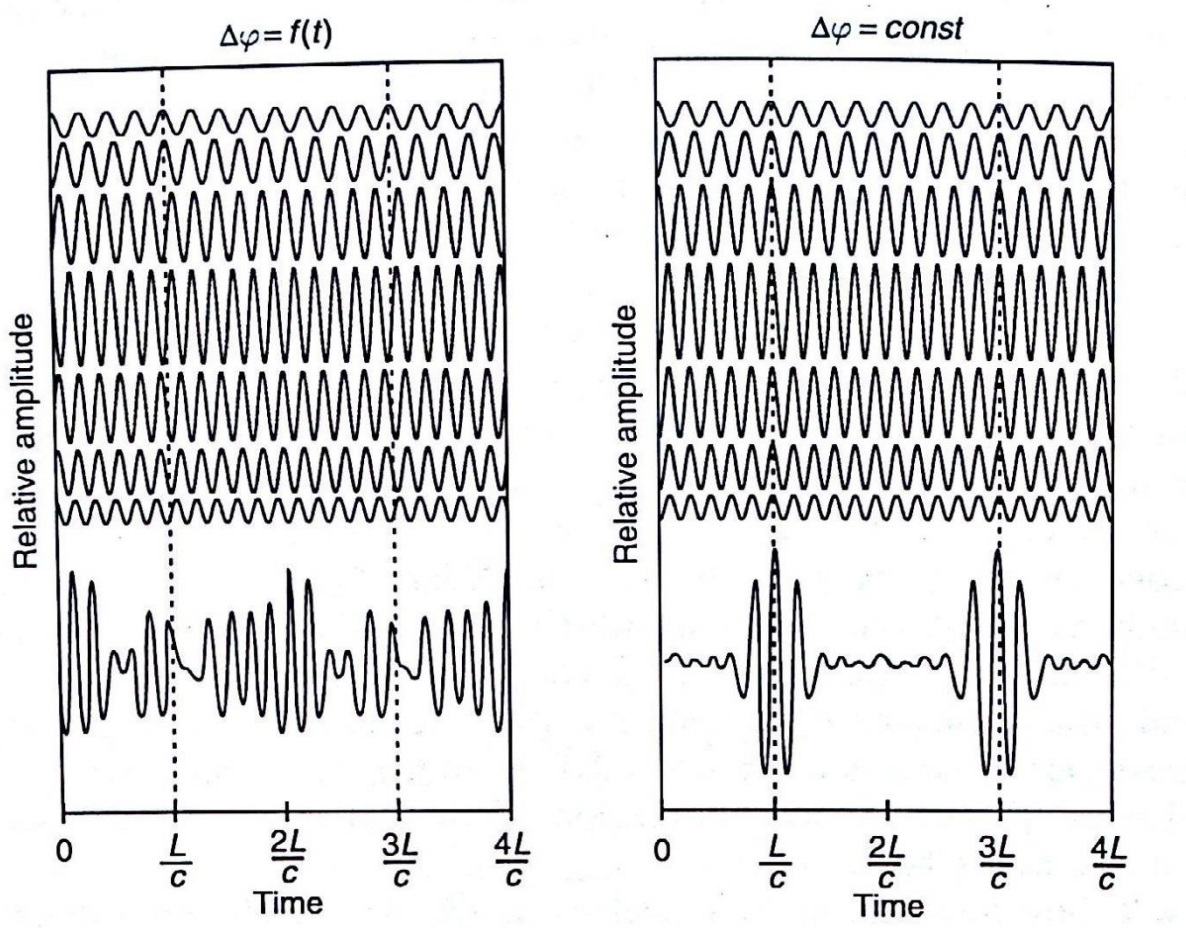

Figure 2.5: The difference between randomly oscillating and locked modes shown as a function of time (*Adopted from* Ref [42])

The longitudinal modes supported by a laser are equally spaced in the frequency domain. If we denote ν_{q+1} as the frequency of the $(q+1)$th mode and so on, the free spectral range (FSR) which is the frequency spacing between two adjacent longitudinal modes, is given by

$$\nu_{FSR} = \nu_{q+1} - \nu_q = \frac{c}{2d}. \qquad (2.5.1)$$

Above, d is the total length of the resonator. To write the net electric field of the oscillating modes we define the difference between the angular frequencies of two adjacent modes is ω_F. The net electric field becomes

$$E(t) = \sum_{q=0}^{M-1} E_q \exp(i(\omega_0 + q\omega_F)t + i\varphi_q(t)), \qquad (2.5.2)$$

where E_q is the amplitude, and $\varphi_q(t)$ is the phase of the qth mode. ω_0 is the reference frequency. To analyze the mode–locking condition $\varphi_q(t)$ for all q's must be zero or constant.

If the phase associated with each mode is constant, then obtain a periodic pulse train as can be seen from Fig. 2.5, and the net electric field becomes

$$E(t) = E_0 \exp(i\omega_0 t) \frac{\sin\left(\frac{M\omega_F t}{2}\right)}{\sin\left(\frac{\omega_F t}{2}\right)}. \quad (2.5.3)$$

Here, M is the number of modes that are oscillating [39]. In a typical mode–locked laser, based on a tunable gain medium, several hundred thousand modes would be locked in phase. The pulse width can be determined from

$$\tau_{pulse} = \frac{1}{M}\left(\frac{2\pi}{\omega_F}\right) = \frac{T_R}{M}, \quad (2.5.4)$$

where T_R is the cavity round–trip time or equivalently, the time between two consecutive mode locked pulses. The pulse width that can be obtained from a gain medium is bounded by the gain bandwidth ($\Delta\nu$). To achieve a pulse width in this limit, the spectral phase must be independent of the frequency as is required for mode locking and the time–bandwidth product must be at its minimum value for a given temporal shape. As an example, the time–bandwidth product is

$$\Delta\nu \cdot \tau_p = 0.315 \quad (2.5.5)$$

for a transform–limited $sech^2$ temporal shape.

There are multiple techniques to achieve mode–locking such as using a modulator, saturable absorber and so on. In general, there are two types of mode–locking mechanisms; active and passive mode–locking. In active mode locking, a modulator is introduced into the laser cavity to obtain pulsed operation. Modulation frequency has to be comparable with the free spectral range (FSR) of the cavity to accomplish continuous wave mode–locking. Modulator is driven by an electronic circuit, therefore; the modulation frequency is controlled by external electronics. In passive mode–locking, a saturable absorber is used. The transmission characteristics of a saturable absorber are intensity dependent. When the incident intensity is large, the transmission also increases. Hence, a larger–intensity beam sees much less loss inside the resonator as opposed to a low–intensity beam. Hence, when a saturable absorber is added to a cavity, the resonator has the tendency to operate in pulsed mode, either Q–switched or mode–locked, to attain higher intensities and to lower the overall loss. Typically, pulsed operation with a saturable absorber requires an initiation method, such a slight displacement of one of the end mirrors.

2.5.1 Kerr–Lens Mode–Locking (KLM)

Kerr–lens mode–locking is a novel passive mode–locking technique. Kerr–lens mode locking was first demonstrated in Ti:Sapphire laser in 1991 by W. Sibbett and his group [11]. After its demonstration, the technique has been applied to several other laser systems [25, 43-46]. To understand the Kerr–Lens mode–locking mechanism, the Kerr effect needs to be investigated. The Kerr effect refers to the intensity dependence of the refractive index and can be expressed in equation form as

$$n = n_0 + n_2 I. \tag{2.5.1.1}$$

Here, n_2 is the nonlinear refractive index in units of cm^2/W. In the case of a Gaussian intensity profile, the center of the beam sees a higher index in comparison with the edges. This resembles a converging lens and leads to the self–focusing of the beam.

To initiate Kerr–lens mode–locking in a laser cavity, the nonlinear refractive index of the gain medium must be positive. If the nonlinear refractive index is positive and if the focusing around the gain medium is properly adjusted, a high–intensity beam undergoes self–focusing and overlaps better with the pump beam. This increases the gain of the oscillating laser beam. Hence, by adjusting the focusing around the gain medium, Kerr–induced focusing can be initiated to favor the mode–locked operation of the laser. . Below the critical power (P_{cr}), given by

$$P_{cr} = \frac{\alpha\lambda^2}{8\pi n_0 n_2}, \tag{2.5.1.2}$$

stable Kerr–lens mode–locking operation can be obtained. In the Eq. 2.5.1.2 α is a unitless factor and λ is the wavelength of the laser. Above the critical power, strong self–focusing may lead to pulse instabilities and limit the maximum energy that can be generated per pulse.

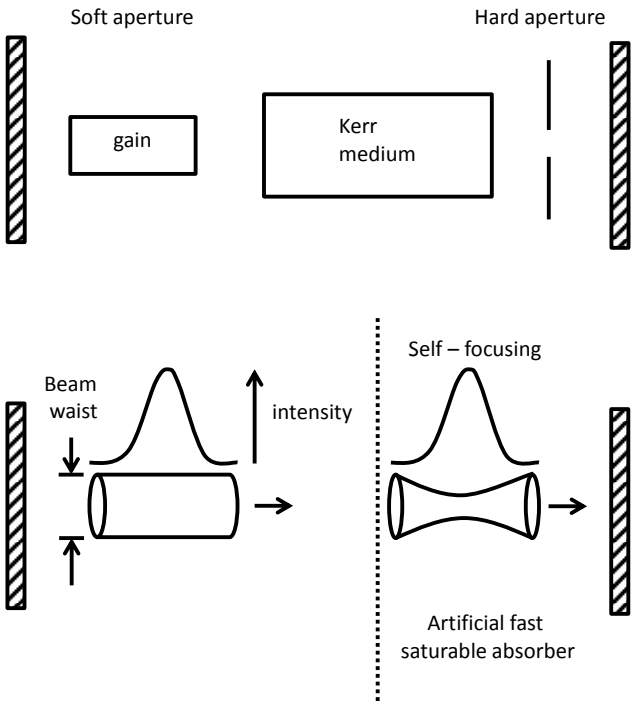

Figure 2.6: Kerr–effect inside the Kerr medium (Adopted *from* Ref [47]).

Kerr–lens mode–locking can be modeled as a fast saturable absorber [48]. The master equation for fast saturable absorber is given as

$$\frac{1}{T_R}\frac{\partial}{\partial T}a = (g - l)a + \left(\frac{1}{\Omega_f^2} + jD\right)\frac{\partial^2}{\partial t^2}a + (\gamma - j\delta)|a|^2 a, \qquad (2.5.1.3)$$

where a is the normalized mode amplitude, and $|a|^2$ gives the instantaneous power. D is the group delay dispersion parameter, Ω_f is the gain bandwidth, g and l are gain and loss parameters, respectively. T_R is the cavity round trip time and T is a long-time parameter of the order of the cavity round trip time.

In Eq. 2.5.1.3, δ is the Kerr–coefficient given by

$$\delta = \frac{2\pi}{\lambda}\frac{n_2 L}{A_{eff}}. \qquad (2.5.1.4)$$

Above, L is the length of the gain medium, λ is the carrier wavelength, A_{eff} is the effective cross–sectional area of the beam. The steady state solution of Eq. 2.5.1.3 is;

$$a(t) = A_0 \mathrm{sech}^{(1+j\beta)}\left(\frac{t}{\tau}\right). \qquad (2.5.1.6)$$

In Eq. 2.5.1.6 β is the chirp parameter.

It can be shown that a nearly chirp–free solitary pulse output can be obtained from a Kerr–lens mode–locked laser, where the pulse energy W and group delay dispersion (GDD) parameter D satisfy

$$W = \frac{4|D|}{\tau\delta}. \qquad (2.5.1.10)$$

Note that as the pulse energy increases, self–phase modulation in the gain medium increases (assuming that the pulse width remains the same) and more negative GDD is needed to balance the Kerr nonlinearities.

As can be seen from Fig. 2.6, there are different ways to achieve Kerr lensing inside a resonator. One of them is called the soft aperture Kerr lensing. Here, the pump beam creates a gain profile which acts as a soft aperture. This means that when the laser beam undergoes self–focusing, it overlaps better with the pump and sees higher gain. The other case is called hard aperture. In this case, an aperture is placed inside the cavity before one of the end mirrors. When the propagating beam undergoes Kerr lensing, it is focused to a smaller spot and has better transmission through the aperture. Hence, Kerr lensing reduces the loss seen by the intracavity beam when a hard aperture is placed at the correct location within the cavity.

In our experiments, by arranging the arm lengths and optimizing the positions of the cavity curved mirrors, the pump beam is focused to a tighter focus than the laser beam. Therefore, femtosecond pulse generation in our case was based on soft aperture Kerr–lens mode–locking.

2.5.2 Group Delay Dispersion (GDD)

In the generation of ultrashort optical pulses, an important problem involves the reduction of phase distortion effects. To analyze the problem, we can start with the Taylor expansion of the phase around a central frequency (ω_0) as given by

$$\varphi(\omega) = \varphi(\omega_0) + \left(\frac{d\varphi}{d\omega}\right)_{\omega_0}(\omega - \omega_0) + \frac{1}{2}\left(\frac{d^2\varphi}{d\omega^2}\right)_{\omega_0}(\omega - \omega_0)^2 + \frac{1}{6}\left(\frac{d^3\varphi}{d\omega^3}\right)_{\omega_0}(\omega - \omega_0)^3. \qquad (2.5.2.1)$$

In Ref [49], a pair of diffraction gratings was shown to compensate the second order (quadratic), $\left(\frac{d^2\varphi}{d\omega^2}\right)_{\omega_0}$, phase distortion. In the paper it was also stated that diffraction gratings

were not sufficient to balance the third order (cubic), $\left(\frac{d^3\varphi}{d\omega^3}\right)_{\omega_0}$, phase distortion. In 1987, Fork *et al.* demonstrated that a combination of prism pairs and diffraction gratings can be used, as shown in Fig. 2.7, to compensate for both quadratic and cubic phase distortions (second order or third order group delay dispersion) [50].

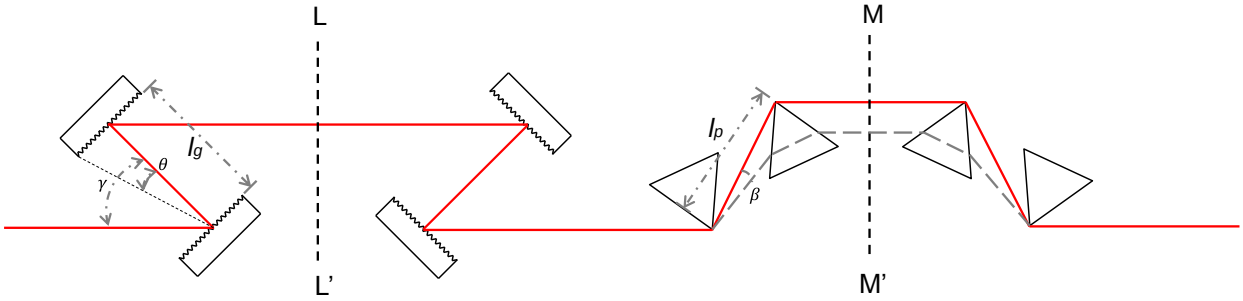

Figure 2.7: Grating and prism pairs for obtaining negative dispersion (*Adopted from* Ref [50])

To balance the second order phase distortion of the pulse inside a resonator, a pair of prisms can be used. The corresponding GDD of the prism pair can be calculated in terms of the derivative of the optical path length P from

$$\frac{d^2\varphi_p}{d\omega^2} = \frac{\lambda^3}{2\pi^2 c^2}\frac{d^2P}{d\lambda^2}. \qquad (2.5.2.2)$$

Here, the derivatives of the optical path length (P) with respect to the vacuum wavelength can be calculated from

$$\frac{d^2P}{d\lambda^2} = 4\left[\frac{d^2n}{d\lambda^2} + (2n - n^{-3})\left(\frac{dn}{d\lambda}\right)^2\right] l_p \sin\beta - 8\left(\frac{dn}{d\lambda}\right)^2 l_p \cos\beta, \qquad (2.5.2.3)$$

where, n is the refractive index of the prism material, l_p is the spacing between the prisms, β is the angular spread in the beam due to dispersion [50]. In our mode–locked laser design, we did not consider and optimize the third order phase distortion effects. As the pulsewidth gets shorter and the bandwidth becomes larger, the cubic distortions must be balanced as well. Third order phase distortion compensation with a prism pair can be accomplished by using the following equations:

$$\frac{d^3\varphi_p}{d\omega^3} = \frac{-\lambda^4}{4\pi^2 c^3}\left(3\frac{d^2P}{d\lambda^2} + \lambda\frac{d^3P}{d\lambda^3}\right) \qquad (2.5.2.4)$$

$$\frac{d^3P}{d\lambda^3} = 4\frac{d^3n}{d\lambda^3} l_p \sin\beta - 24\frac{dn}{d\lambda}\frac{d^2n}{d\lambda^2} l_p \cos\beta. \qquad (2.5.2.5)$$

For example, a pair of fused silica prisms with a separation distance of 30 cm, as we employed in our cavity design, will provide the GDD curve as a function of wavelength shown in Fig. 2.8.

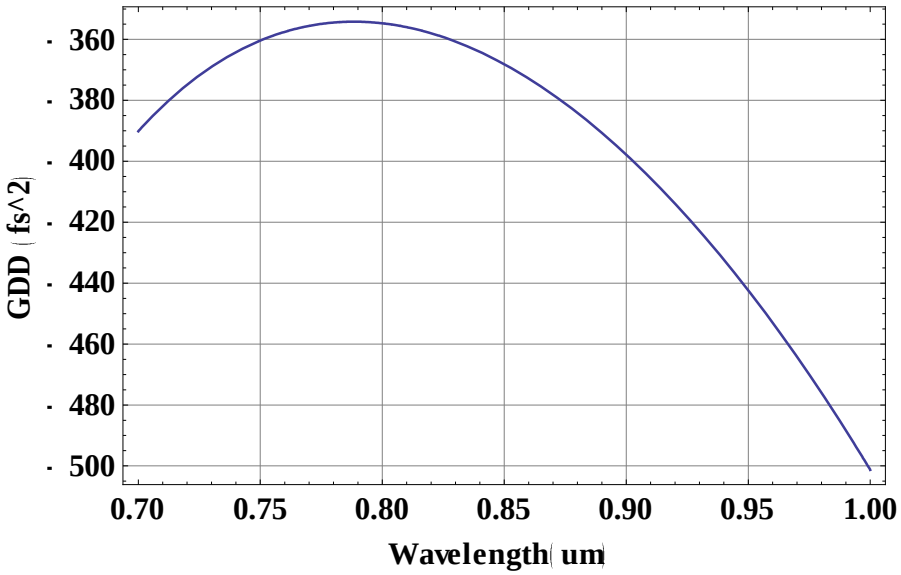

Figure 2.8: GDD curve of a prism pair made of fused silica at a 30 cm separation distance.

Using a pair of prisms yields the desired nearly flat dispersion curve between 0.8–0.86 μm. To achieve the desired flat dispersion level, we used a pair of prisms in the second part of the mode–locking experiments.

In order to determine the phase distortions arising from each optical component in a laser cavity, we need to know how the refractive index of that medium changes with wavelength. An empirical formula, known as the Sellmeier equation, gives the measured refractive index of a medium as a function of wavelength. In our case, we need to consider the Sellmeier equations for LiSAF crystal [51], air, and fused silica (material of the GMOC and prism pair). The Sellmeier equations are given respectively as follows:

$$n_{c-LiSAF} = \sqrt{1.98448 + \frac{0.00235}{\lambda^2 - 0.10936} - 0.01057\lambda^2} \quad (2.5.2.9)$$

$$n_{a-LiSAF} = \sqrt{1.97673 + \frac{0.00309}{\lambda^2 - 0.00935} - 0.00828\lambda^2} \quad (2.5.2.10)$$

$$n_{Air} = 1 + \frac{5792105\times10^{-8}}{238.0185 - \lambda^{-2}} + \frac{167917\times10^{-8}}{57.362 - \lambda^{-2}} \quad (2.5.2.11)$$

$$n_{Fused\ Silica} = \sqrt{1 - \frac{0.6961663\lambda^2}{\lambda^2 - 0.0684043^2} - \frac{0.4079426\lambda^2}{\lambda^2 - 0.1162414^2} - \frac{0.8974794\lambda^2}{\lambda^2 - 9.896161^2}} \quad (2.5.2.12)$$

The refractive index variation of LiSAF, air and fused silica are given in Figs. 2.9 and 2.10.

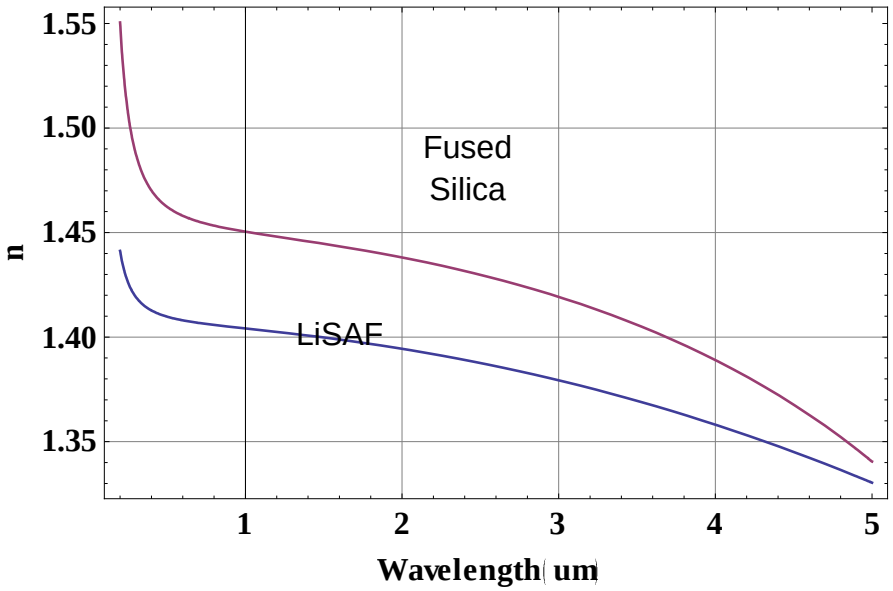

Figure 2.9: Refractive index variation of LiSAF and fused silica as a function of wavelength

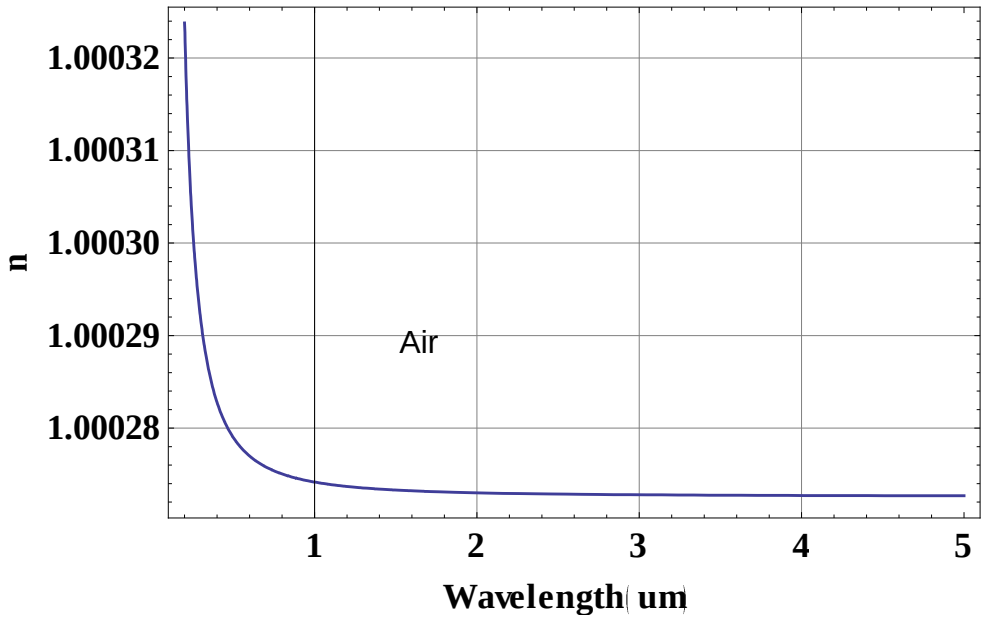

Figure 2.10: Refractive index variation of air as a function of wavelength

Figures 2.11 a–c show the calculated GDD for a LiSAF crystal, air, and a fused silica slab by using the GDD formula for a slab [50]. The calculation was done in the 700–1300 nm wavelength range.

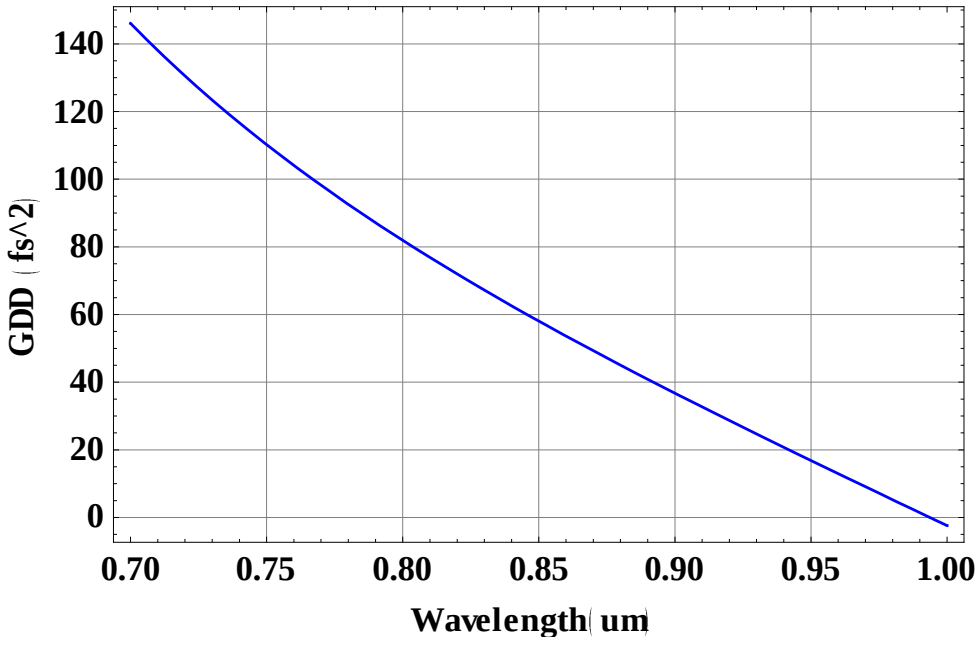
GDD (fs^2)
140
120
100
80
60
40
20
0
0.70
0.75
0.80
0.85
0.90
0.95
1.00
Wavelength(um)

a)

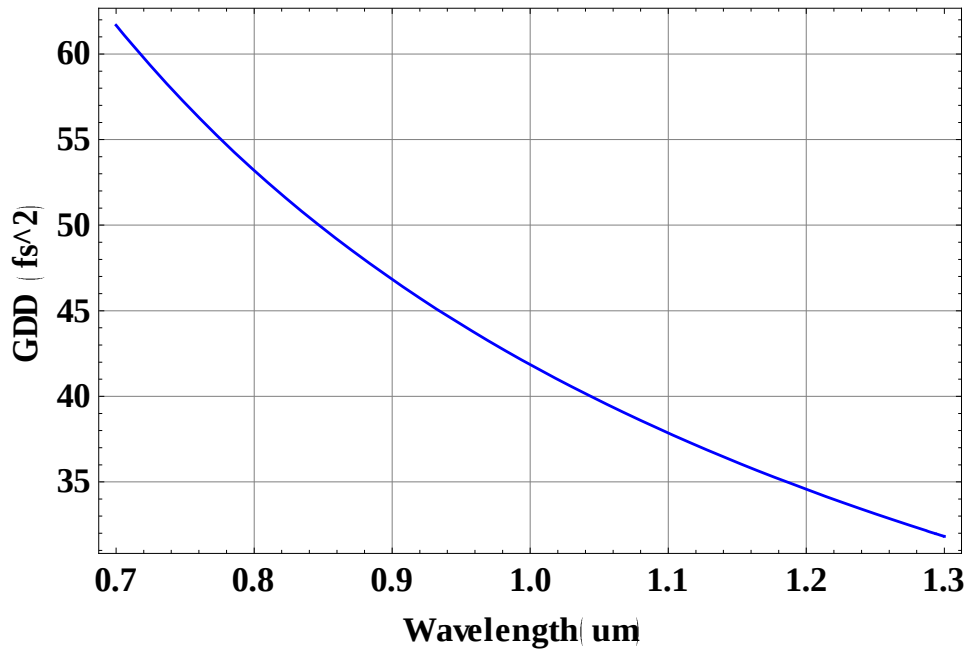
GDD (fs^2)
60
55
50
45
40
35
0.7
0.8
0.9
1.0
1.1
1.2
1.3
Wavelength(um)

b)

c)

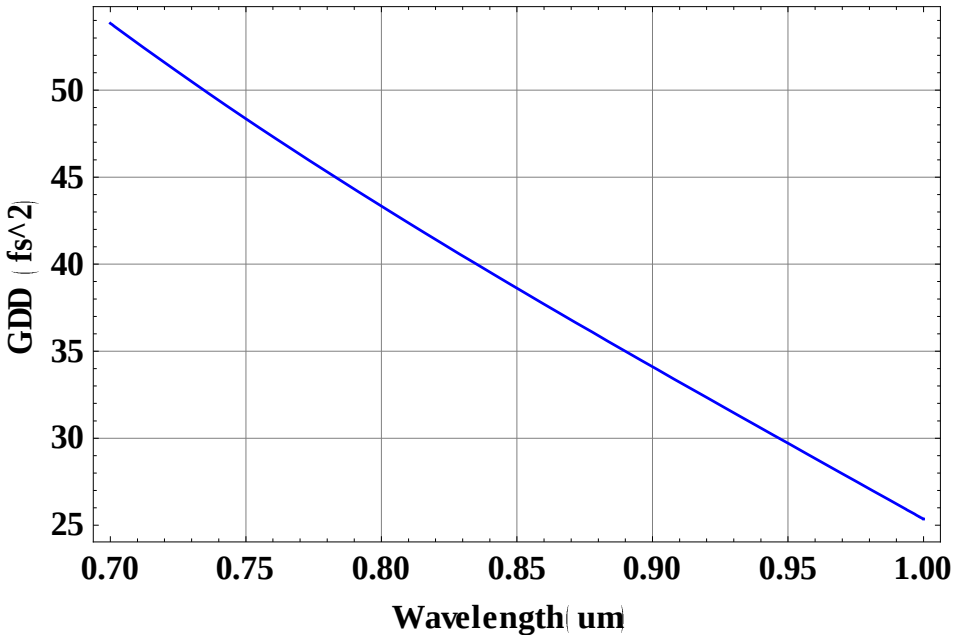

Figure 2.11: Calculated variation of GDD between 700 and 1300 nm for a) LiSAF (6 mm) b) Air (2.5 m) c) Fused Silica Slab (1.2 mm)

Another important method for the compensation of phase distortions involves the use of double–chirped mirrors (DCM) [52]. Double–chirped mirrors are designed to be high reflective in the gain range and provide negative dispersion. The amount of negative dispersion provided by the DCM depends on the coating materials and the layer thicknesses. In our laser setup, DCMs were also included for dispersion compensation.

3 EXPERIMENTAL SETUP AND RESULTS

3.1 Experimental Setup

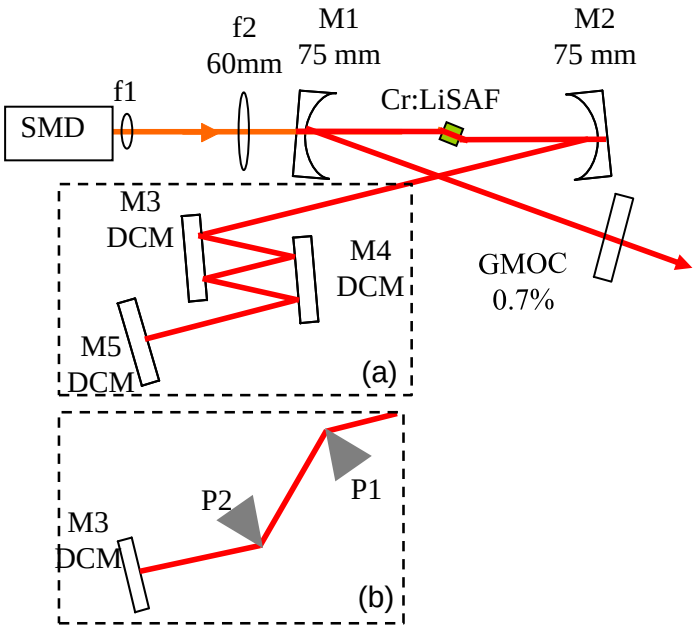

Figure 3. 1: Schematic of Cr:LiSAF experimental setup that was used in mode–locking experiments. (a) DCM mirrors and/or a fused silica prism pair (b) was used for dispersion compensation.

For dispersion compensation, DMC mirrors and/or a fused–silica prism pair has been employed. The prismless cavity configuration is shown in Fig. 3.1 (a). M1 and M2 are curved mirrors, each with a radius of curvature of 75 mm. The mirrors have high reflectivity (HR) at the gain bandwidth (between ~750–950 nm), and have high transmission around the pump wavelength (660 nm). To reduce the reflection losses of the horizontally polarized input light, the crystal is placed at Brewster's angle (54.4^{o}) inside a copper holder without any cooling mechanism. The Cr:LiSAF crystal has a length of 6 mm and a Cr dopant concentration of 1.5%. M3–M5 are commercially available flat DCM mirrors with a dispersion of –50 fs^2 per bounce. The net cavity dispersion is estimated to be around –50 fs^2.

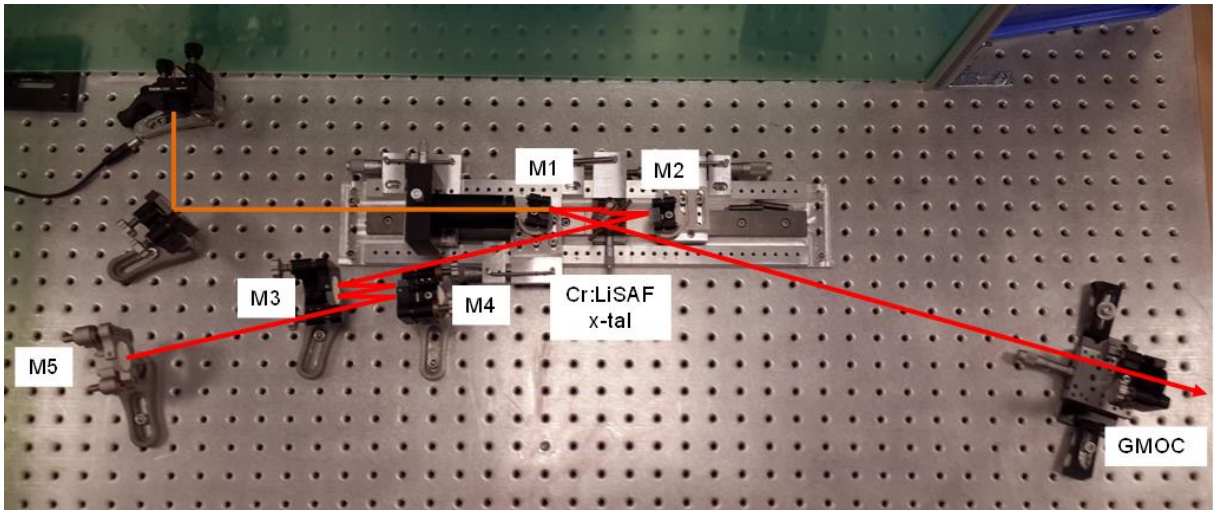

Figure 3.2: Picture of the prismless Cr:LiSAF cavity

Figure 3.2 shows a photo of the laser cavity for the prsimless cavity configuration. In Fig. 3.1, 3.2, and 3.3, the orange line shows the path of the pump light and the red line shows the path of the laser beam. The length of the output coupler (OC) arm and the high reflector (HR) arm are ~50 cm and ~65 cm, respectively.

In Fig 3.1 (b), DCM mirrors in the dashed box are replaced with a pair of Brewster cut fused silica prisms to obtain a nearly flat group delay dispersion around 850 nm. The distance between the prisms is 30 cm, corresponding to about ~–350 fs^2 of dispersion (more details can be found in Chapter 2). M1–M2 are DCM mirrors with –60 fs^2 dispersion, where as M5 is a DCM mirror with –50 fs^2 dispersion. In this configuration, HR arm length was ~60 cm and OC arm length was the same as in the prismless configuration (~50 cm). We note here that, we have also applied external dispersion compensation (about –120fs^2 using M4–M7), to limit pulse broadening effects from material dispersion (dispersion of OC, air, and the beam splitter in the autocorrelator). The external dispersion compensation mirrors can be seen in Fig. 3.3 (M4–M7). In the next section, we will present results obtained by using both cavity configurations.

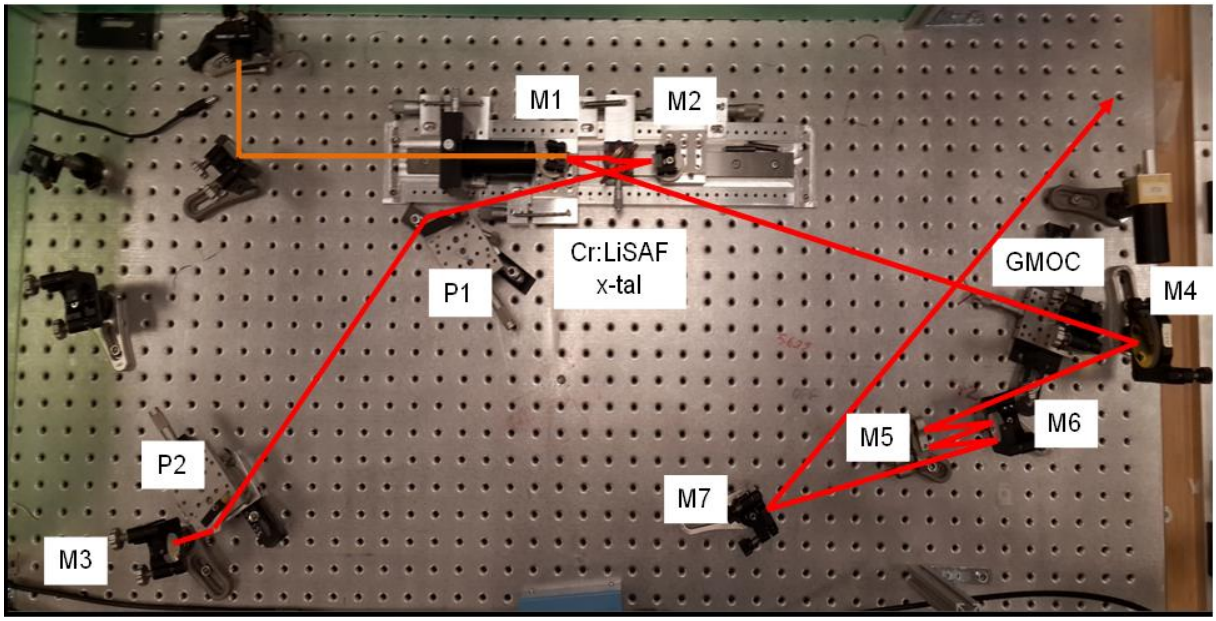

Figure 3.3: Picture of the Cr:LiSAF cavity with a fused silica prism pair and autocorrelation path (M4–M7)

3.2 Mode–Locking Results from the Prismless Cr:LiSAF Laser

This section presents the cw mode–locking results of the SMD pumped prismless Cr:LiSAF laser cavity. The cavity design can be seen in Fig. 3.1 (a). The cw lasing threshold of the configuration was around 20 mW, and the laser operated only in pure cw regime for pump powers up to 50 mW. The slope efficiency for cw regime was 20% (Fig. 3.4). Above 50 mW of pump power, Cr:LiSAF cavity could generate ultrashort pulses, operating in Kerr–lens mode–locking regime by slightly shaking one of the cavity end mirrors. The maximum available pump power is 135 mW, and up to 100 mW of pump power, Cr:LiSAF laser has supported stable mode–locked operation. Representative stable mode–locking results in this region with nearly transform–limited pulse widths are shown in Fig. 3.5 (a)–(c). Above 100 mW of pump power, the laser supported bistable operation regime, where ultrashort pulses with different optical spectrum, output power and chirp have been observed (second mode–locked part in Fig. 3.4). However, we could choose the operation point of the laser by fine adjustment of the output coupler position. The spectral intensities and the corresponding autocorrelation traces for this regime can be seen from Fig. 3.6 (a)–(e). For all mode–locked regimes above 100 mW input pump power, the pulses from the Cr:LiSAF laser were not transform–limited. In other words, the output pulse is a chirped soliton, and the pulse is distorted in time domain. As a solution, a pair of prisms and DCM mirrors was added outside

of the cavity. However, shorter pulses could not be achieved. For example, at 135 mW pump power, the obtained optical spectrum from the Cr:LiSAF laser has a FWHM of around 50 nm which supports 15–fs long pulses, assuming transform limited operation. However, the measured pulse width was 27 fs, with a corresponding time–bandwidth product was 0.57. Table 3.1 lists all the results obtained from the prismless Cr:LiSAF laser design at different input power levels.

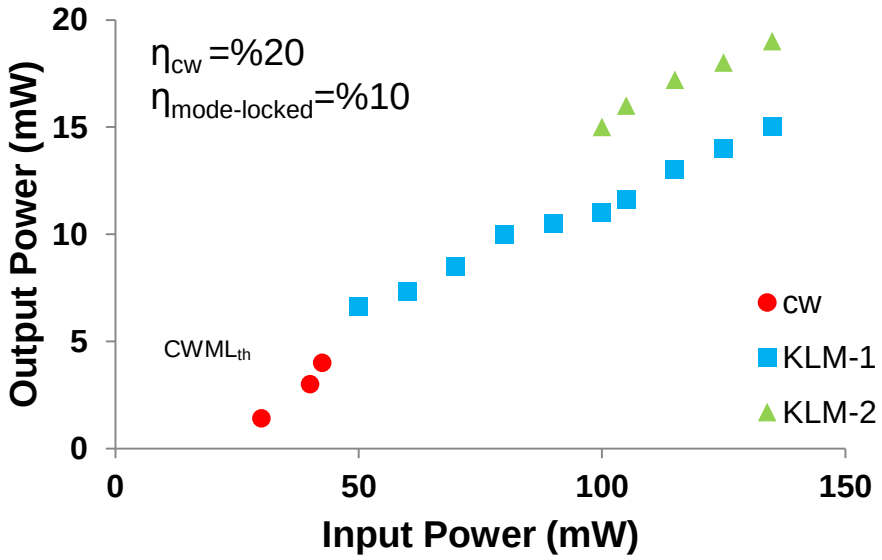

Figure 3.4: The laser efficiency curves taken with the prismless Cr:LiSAF laser cavity. Different regimes of operation (cw and mode–locking) have been. Observed at different pump power levels.

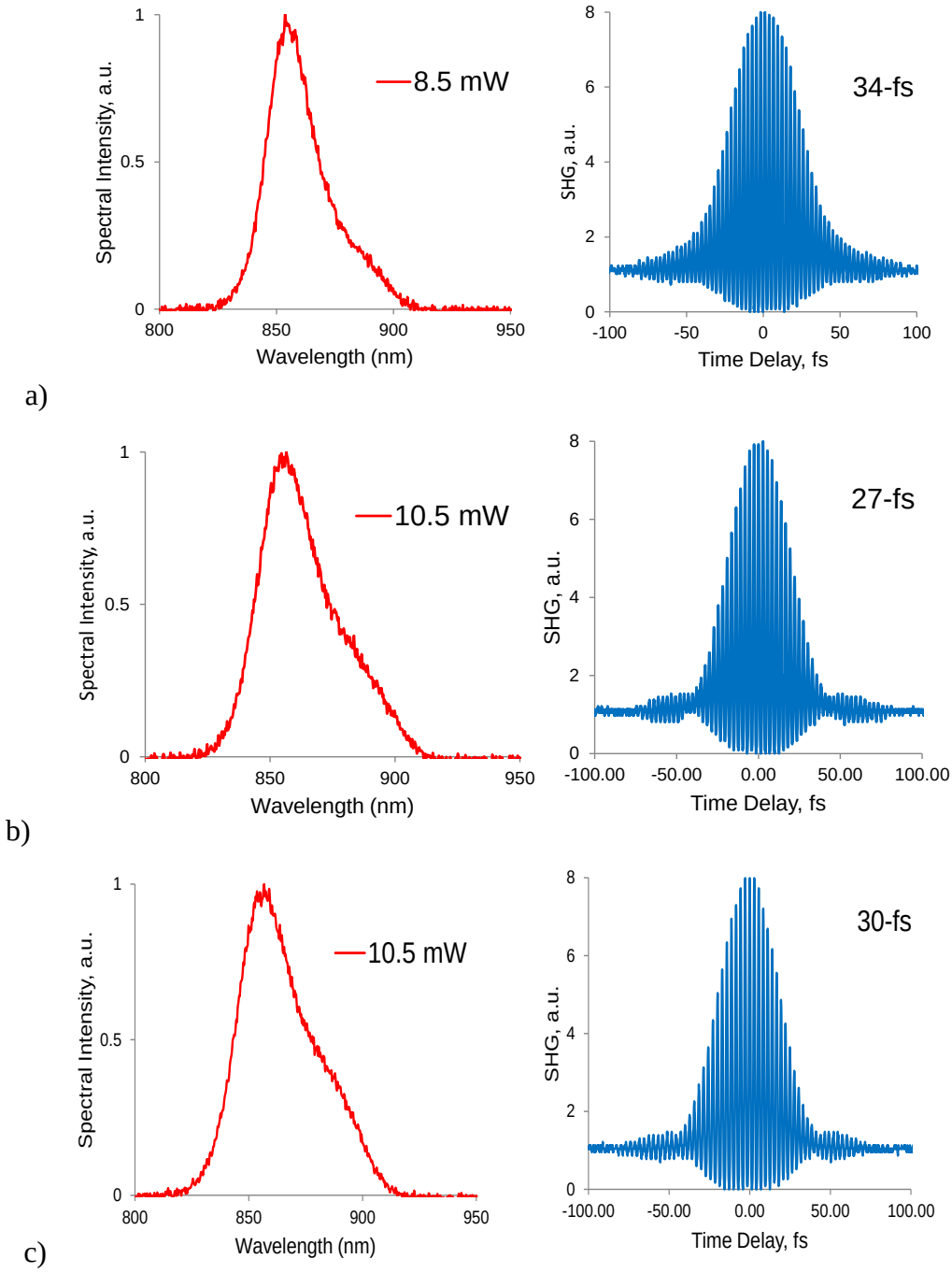

Figure 3.5: Spectrum and autocorrelation traces obtained from the KLM Cr:LiSAF laser at the incident pump powers of a)70 mW, b) 85 mW, and c) 95 mW.

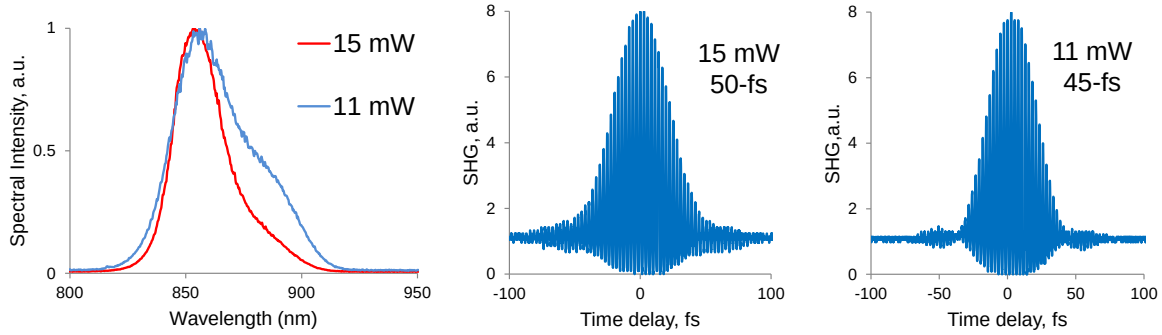
Spectral Intensity, a.u.
Wavelength (nm)
15 mW
11 mW
SHG, a.u.
Time delay, fs
15 mW
50-fs
SHG,a.u.
Time delay, fs
11 mW
45-fs

a)

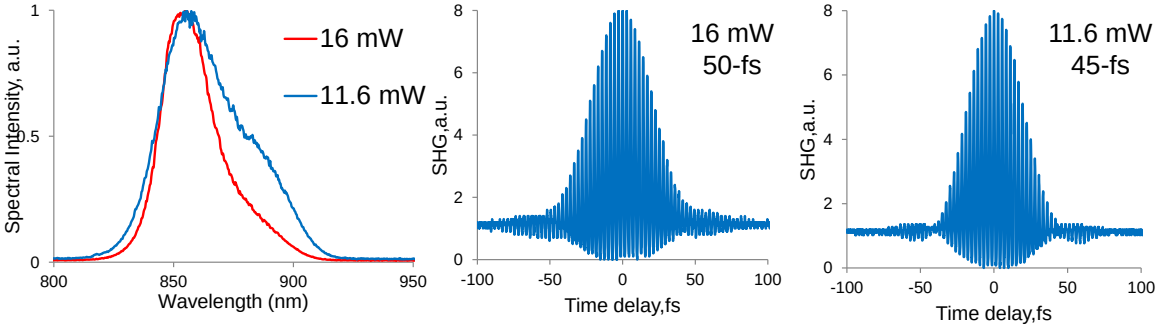
Spectral Intensity, a.u.
Wavelength (nm)
16 mW
11.6 mW
SHG,a.u.
Time delay,fs
16 mW
50-fs
SHG,a.u.
Time delay,fs
11.6 mW
45-fs

b)

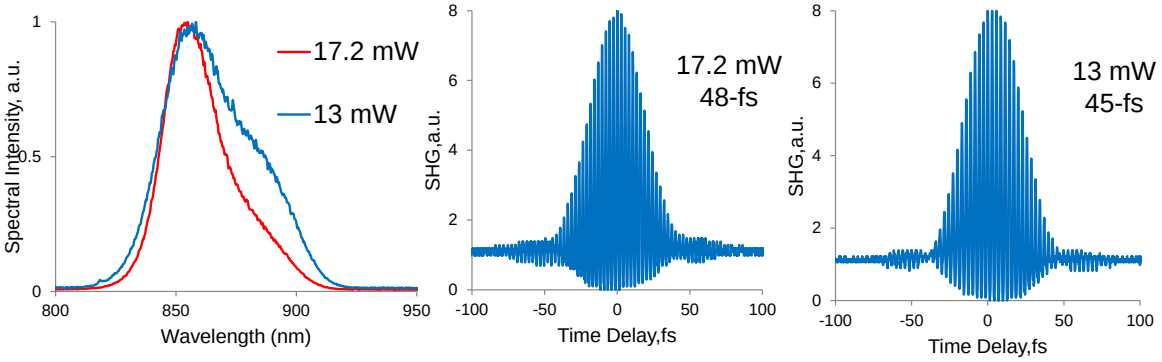
Spectral Intensity, a.u.
Wavelength (nm)
17.2 mW
13 mW
SHG,a.u.
Time Delay,fs
17.2 mW
48-fs
SHG,a.u.
Time Delay,fs
13 mW
45-fs

c)

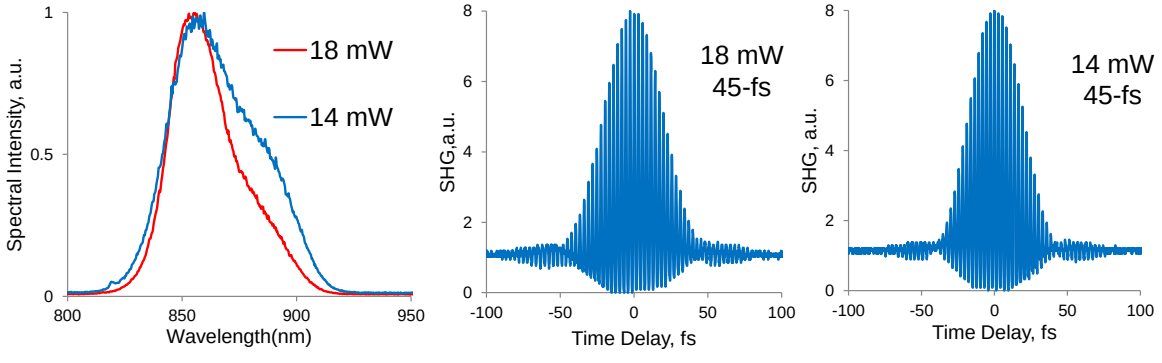
Spectral Intensity, a.u.
Wavelength(nm)
18 mW
14 mW
SHG,a.u.
Time Delay, fs
18 mW
45-fs
SHG, a.u.
Time Delay, fs
14 mW
45-fs

d)

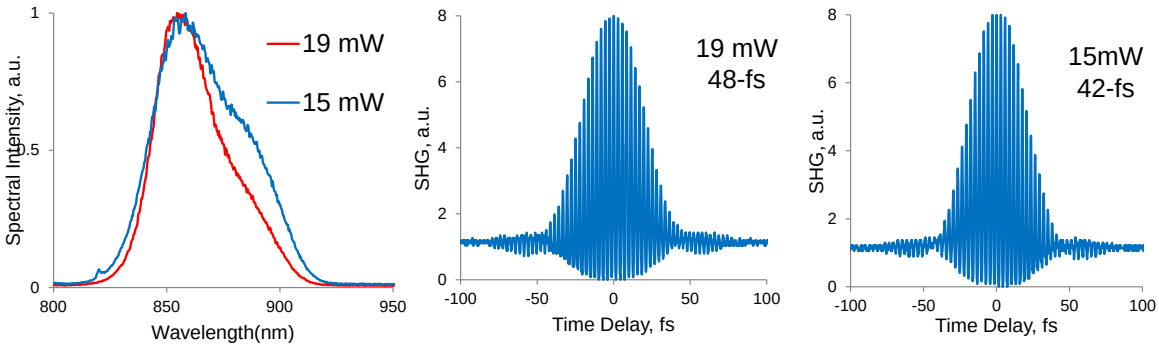

e)

Figure 3.6: Spectral intensities for bistable mode–locking regimes from the KLM Cr:LiSAF laser taken at incident pump powers of a) 100 mW, b) 105 mW, c) 115 mW, d) 125 mW, and e) 135 mW.

Table 3.1: List of output powers, pulse energies and peak powers obtained from the KLM Cr:LiSAF laser taken at different incident pump power levels. Time–bandwidth product, optical spectral width ($\Delta\lambda$) and pulse width (τ_p) values are also shown.

Incident pump power (mW)	Laser output power (mW)	$\Delta\lambda$ (nm)	τ_p (fs)	$\Delta\nu$ (THz)	$\tau_p.\Delta\nu$	Peak power (kW)	Pulse energy (pJ)
70	8.5	24	34	9.8	0.333	1.9	71.4
80	10.5	28	29	11.4	0.331	2.7	88.2
85	10.5	30	29	12.3	0.356	2.7	88.2
95	11	34	30	13.9	0.417	2.7	92.4
100	15	26	32	10,7	0,346	3.5	126
100	11	36	29	14,8	0,426	2.8	92.4
105	16	27	32	11,1	0,359	3.7	134.4
105	11.6	38	29	15,6	0,449	3.0	97.4
115	17.2	29	31	11,9	0,364	4.1	144.5
115	13	44	29	18,1	0,521	3.3	109.2
125	18	31	29	12,7	0,365	4.6	151.3
125	14	45	29	18,5	0,532	3.6	117.7
135	19	35	31	14,4	0,440	4.5	160
135	15	49	27	20,1	0,542	4.1	126

Fig. 3.7 shows the measured variation of laser output spectrum as a function of incident pump power. Calculated total GDD level of the cavity is also shown. The total dispersion is –50 to –100 fs^2 around 850 nm. As can be seen the GDD bandwidth of the commercial DCM mirrors limit the obtainable pulse widths.

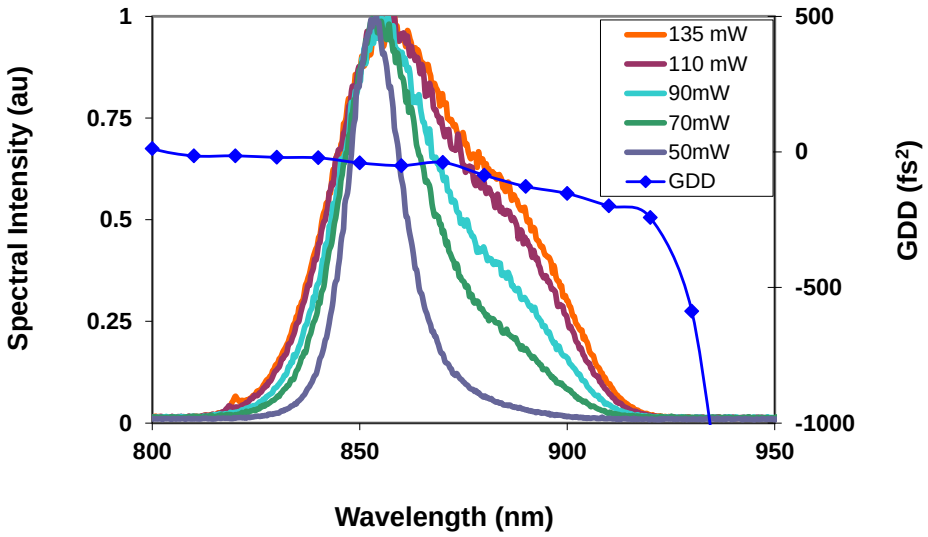

Figure 3.7: Measured variation of optical spectra of the pulses (normalized) taken at different incident pump power levels. Calculated total GDD of the cavity is also shown.

The shortest output pulses from the prismless Cr:LiSAF cavity design were obtained at an incident pump power of 80 mW. The optical spectrum is centered around 850 nm with a FWHM of 28 nm. The corresponding pulse width was measured with an interferometric autocorrelator (see Appendix A), and the autocorrelation trace can be seen in Fig. 3.8 (c).The measured pulsewidth is 29 fs (assuming $sech^2$ pulse shape), with time–bandwidth product of 0.331 (Fig. 3.8 (a)). The repetition rate was around 119 MHz, and the measured radio frequency (RF) spectrum of the pulse train had a clean RF peak without any side bands (Fig. 3.8 (d)). The laser output average power was 10 mW, which corresponds to a pulse energy of 85 pJ and a peak power of 4 kW. The output beam shape of the laser was TEM_{00} when KLM was initiated. Otherwise, it was not a circularly symmetric beam profile as can be seen from Fig. 3.8 (b).

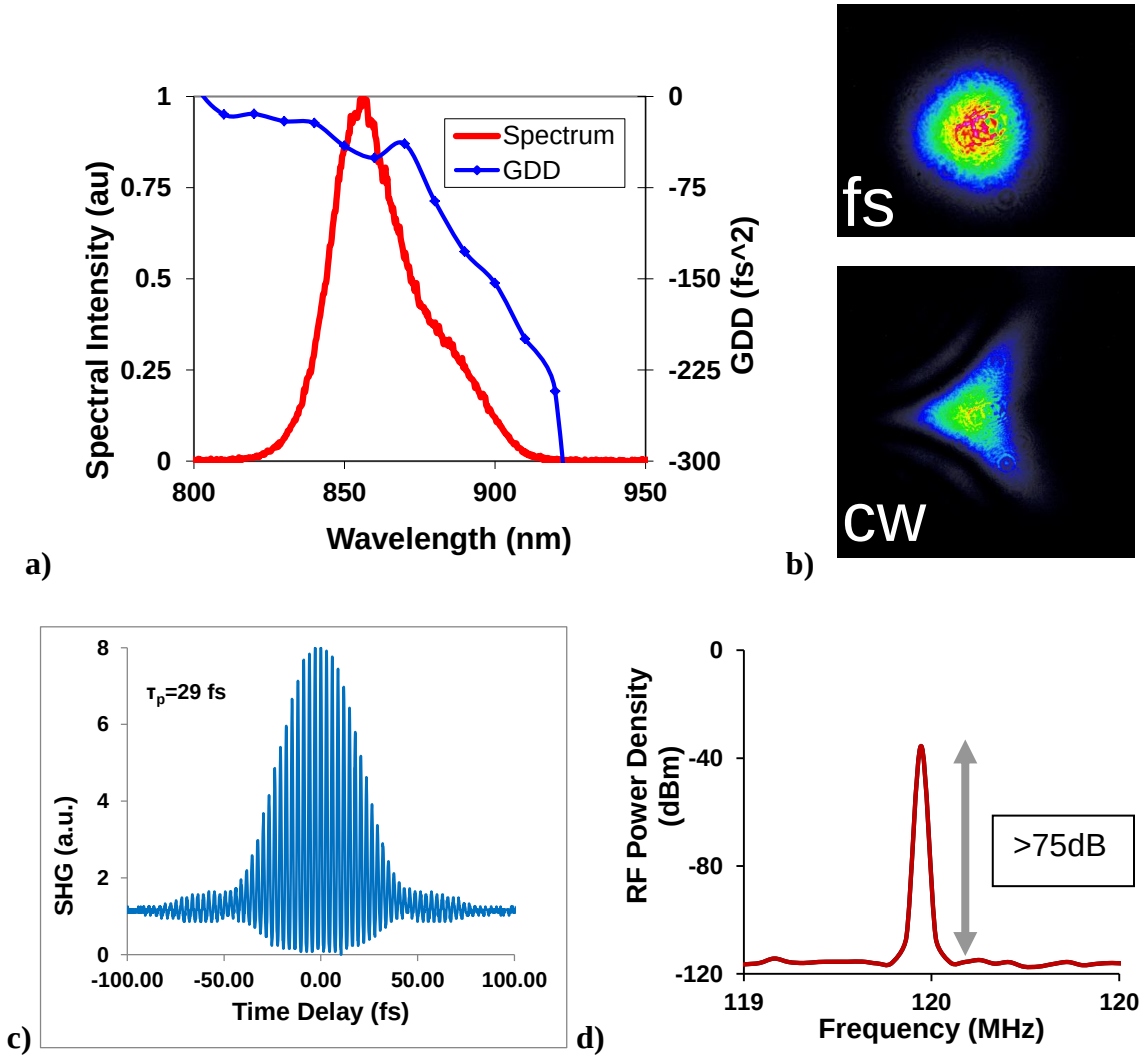

Figure 3.8: a) The spectral intensity of the shortest pulse output. b) Spatial intensity distribution of the laser for mode–locked and cw output cases. c) The interferometric autocorrelation trace at 80 mW incident pump power. d) Radio frequency (RF) spectrum of the corresponding pulse train

As we discussed earlier, use of the GMOC mirror enables robust and stable KLM operation. Moreover, it removes the necessity to operate the Cr:LiSAF laser at the edge of the stability range. Calculated stability range of the prismless Cr:LiSAF cavity is given in Fig. 3.9 (see Appendix B for details). Experimentally, we have obtained the best KLM results at a Cr:LiSAF crystal-M2 separation of 0.033 m. Note that this corresponds to a point near the center of the stability range, which enables efficient laser operation as well as higher output beam quality. As additional information about this configuration, it was not possible to obtain stable KLM operation by using regular output couplers. The same output coupling level as

GMOC (0.7 %) as well as lower output coupling had been tried, and stable KLM could not been observed.

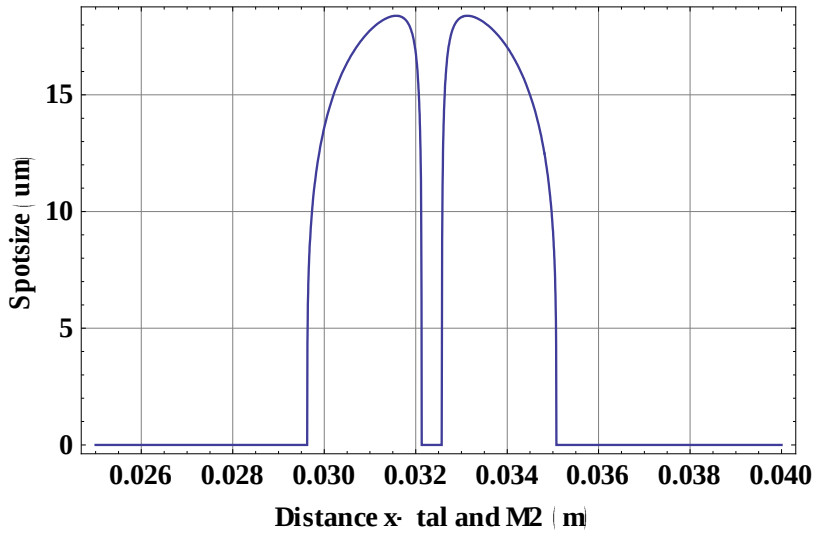

Figure 3. 9: Calculated variation of the beam waist inside the Cr:LiSAF crystal as a function of the distance between the edge of the crystal and the first mirror.

3.3 Mode–Locked Results with a Pair of Prisms

In this section, we will present mode–locking results obtained using the Cr:LiSAF laser with a fused silica prism pair. Compared to the prismless cavity, in this cavity narrower band DCM mirrors have been removed. Moreover, by playing with the insertion of the prisms we could fine tune the total cavity dispersion. Hence, a broader dispersion bandwith with a fine tuning knob has been obtained in this cavity configuration.

Similar to the prismless cavity, the cw threshold pump power was around 20 mW (Fig. 3.10).For pump powers up to 50 mW purely cw operation is observed from the cavity. Above 50 mW, mode–locked operation could be obtained by shaking one of the cavity end mirrors. Once initiated, the system was quite stable and stayed in mode–locked regime for hours. At the incident pump power of 120 mW, by adjusting the material insertion of the second fused silica prism, it was possible to change output pulse width in the range from 13 fs to 50 fs. For example, around ~8 mm of fused silica material insertion has been applied to obtain the shortest pulses (13 fs).

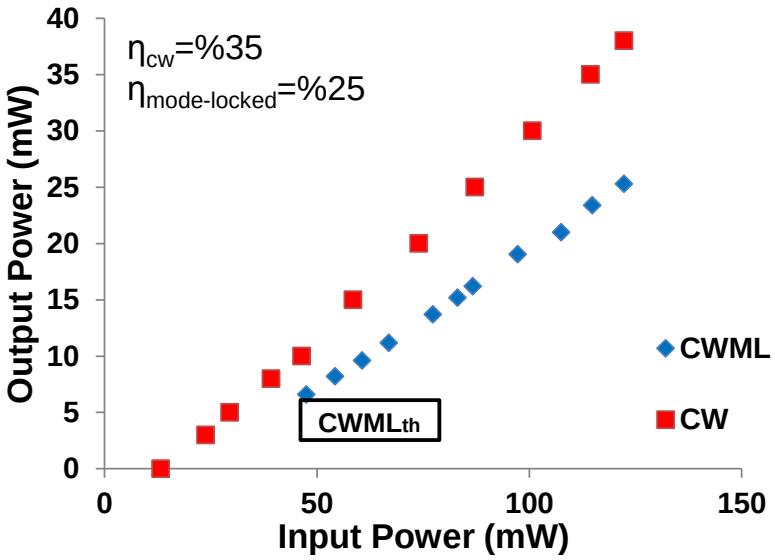

Figure 3. 10: Measured variation of laser output power with incident pump power levels in both cw and mode–locking cases for the KLM Cr:LiSAF with the fused silica prism pair.

The spectral intensity of the best pulse width (13–fs) is shown in the Fig. 3.11 (a). The profile of the spectral intensity was not smooth, hence it is not possible to assume a $sech^2$ pulse shape. As a result, we have calculated the autocorrelation factor for this pulse shape, which is found to be 1.78. The transform limited pulse duration is 11.8 fs and the minimum theoretical time–bandwidth product is 0.45 for this spectral shape. According to these calculated values, the measured pulse width is 13–fs and the time–bandwidth product is 0.5 (slightly above the minimum achievable value of 0.45). The results show that the output pulses were almost transform limited.

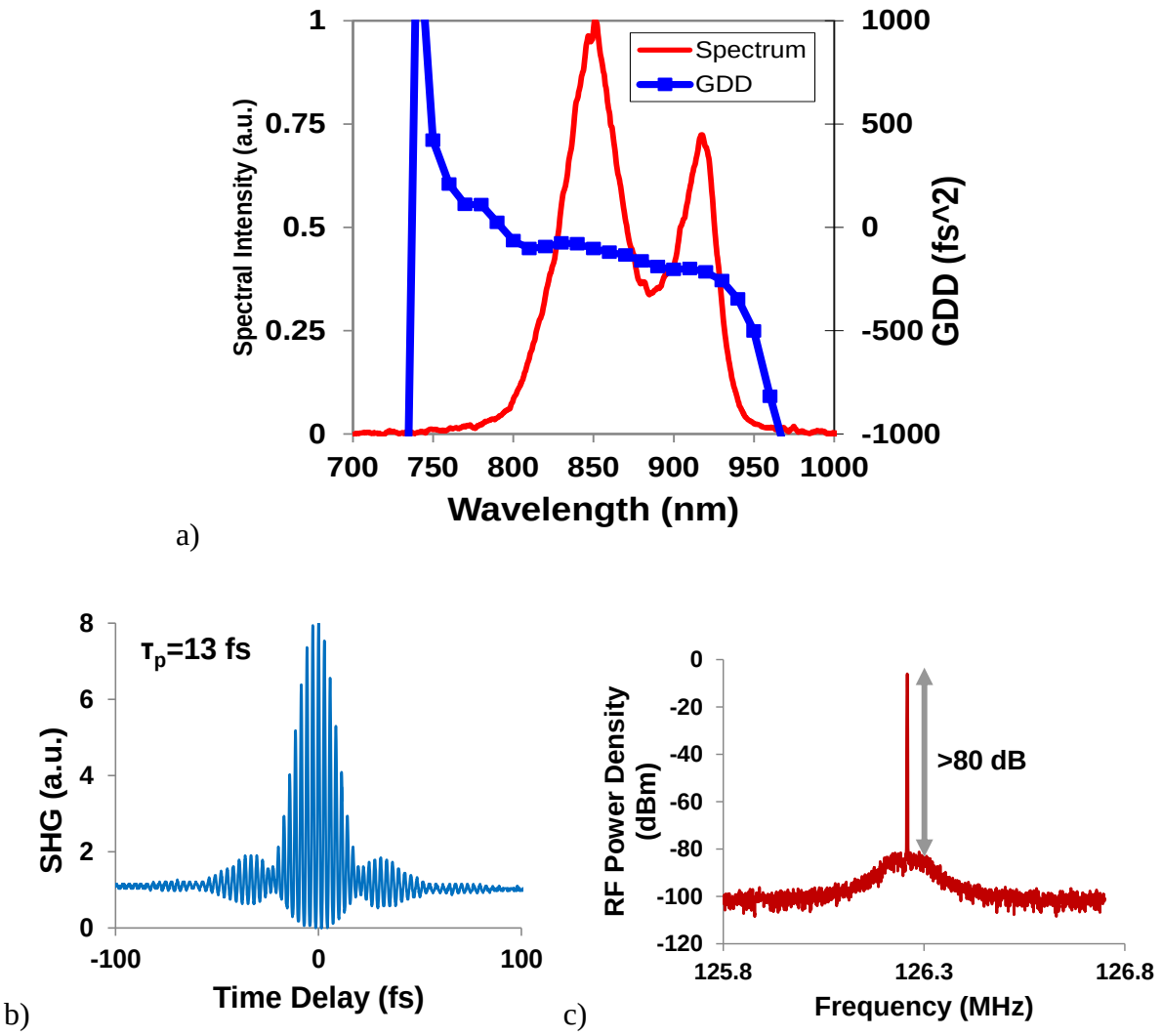

Figure 3. 11: a) The spectral intensity of cw–mode–locked Cr:LiSAF cavity with a pair of prisms. b) The interferometric autocorrelation trace of the given spectral intensity. c) RF spectrum of given pulse train

At the input power 120 mW, the average output power was 25 mW and the corresponding peak power and pulse energies were 14 kW and 200 pJ, respectively. For the measured pulse width, we used an intensity autocorrelation and the corresponding autocorrelation trace is given in Fig. 3.11 (b). The repetition rate was 126 MHz, and the measured radio frequency (RF) spectrum of the pulse train had a clean RF peak without any noise side bands as shown in Fig. 3.11 (c).

We have also tried central wavelength tuning of the femtosecond pulses for this configuration by adding a hard aperture after the second prism. The center wavelength of the

pulses could be tuned smoothly from 840 nm to 870 nm (Fig. 3.12). We believe that the tuning range can be extended further in future studies.

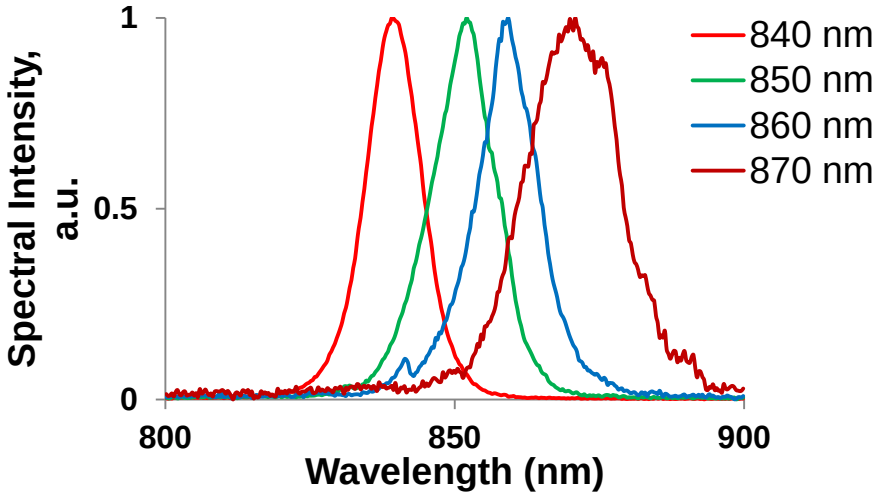

Figure 3. 12: Optical spectrum of femtosecond pulses obtained at different central wavelengths.

Table 3.2: List of pulse widths and spectral widths obtained at different center wavelengths.

λ_c (nm)	$\Delta\lambda$ (nm)	τ_p (fs)	$\Delta\nu$ (THz)
840	11	70	4.6
850	12	65	4.9
860	11	70	4.4
870	19	41	7.5

We note here that, for the Cr:LiSAF cavity with the fused silica prism pair, KLM operation could be obtained also by using regular output couplers (0.75% and 0.15%). However, the pulsewidths were limited to 25–fs level. Moreover KLM operation was less stable due to the increased effect of gain filtering.

4 CONCLUSIONS

In this study, we have demonstrated efficient and robust Kerr–lens mode–locked (KLM) operation of a low–cost single–mode diode pumped Cr:LiSAF laser by using gain–matched output coupler (GMOC) technology. Pulses as short as 13-fs and peak powers as high as 14 kW have been demonstrated. The most important result is that, despite the low nonlinear refractive index of Cr:LiSAF, KLM operation could be sustained for several hours. Moreover, the optical-to-optical conversion efficiency of the system was about an order of magnitude better than previous studies in the literature.

In the case of the prismless configuration, the generated pulse width was 29–fs with 10.5 mW of average output power. The central wavelength of the optical spectrum was at 855 nm with a FWHM of 28 nm. The corresponding time–bandwidth product was 0.331, close to the theoretical value for $sech^2$ pulse shape. The pulse repetition rate was 119 MHz, corresponding to a peak power and pulse energy of 4 kW and 85 pJ, respectively.

KLM operation of the Cr:LiSAF cavity with a pair of fused silica prisms generated pulses as short as 13–fs, at a repetition rate 126 MHz with 25 mW average output power. The output pulse width could be tuned from 13 to 50 fs by changing the material insertion amount of the second prism. The center wavelength of the pulses was around 855 nm. Using the measured spectral intensity of the generated pulses, the calculated minimum time–bandwidth product came to 0.45, which was close to the experimentaly measured value (0.5), confirming that almost transform limited pulse generation was achieved. The peak power and the pulse energy of the pulses were 14 kW and 120 pJ, respectively.

To the best of our knowledge, this is the first demonstration of GMOC technology in mode-locking of Cr:LiSAF lasers. Use of GMOC removes the need to use any additional elements like hard apertures, which introduces additional losses to the resonator. Moreover, unlike most of the earlier KLM studies with Cr:LiSAF, with the help of the GMOC, KLM operation has been achieved near the center of the stability range which optimizes the output beam quality and improves the obtainable average powers. As a result, demonstrated optical-to-optical conversion efficiencies (25%) are an order of magnitude better than what was

achieved earlier (10 fs pulses with 0.27 % efficiency in [20], 12–fs pulses with 0.76% efficiency in [53], 15–fs pulses with 1.5 % efficiency in [44]). This study has also demonstrated that, besides the Ti:Sapphire laser, GMOC technology can successfully be applied to laser materials like Cr:LiSAF with low nonlinear refractive index.

Compared to Ti:Sapphire lasers that require expensive and bulky pump sources ($50k), the Cr:LiSAF laser was compact and inexpensive ($10k). As another advantage of the system, the electrical–to–optical conversion efficiency of Cr:LiSAF laser was around 7 %, which is approximately two orders of magnitude better than today's commercial Ti:Sapphire lasers. These results have shown that, low-cost and efficient Cr:LiSAF lasers with ultrashort pulses have the potential to replace Ti:Sapphire lasers in selected scientific and technological applications.

APPENDIX A : DESIGN OF THE INTERFEROMETRIC AUTOCORRELATOR

The output pulse duration from the Cr:LiSAF laser is as short as 13–fs. For such short durations it is not possible to measure with commercially available detectors or oscilloscopes. In order to characterize these femtosecond durations we built an interferometric autocorrelator. A simple sketch of the autocorrelator can be seen in Fig. A.1 and a picture of it can be seen in Fig. A.2.

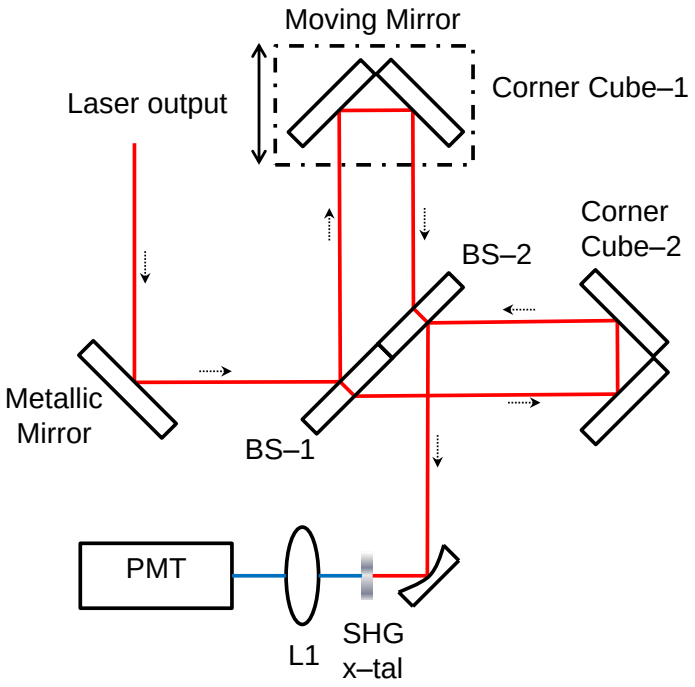

Figure A. 1: Interferometric autocorrelation set – up

Our interferometric autocorrelator simply consists of a Michelson interferometer, a second harmonic crystal and a fast detector (PMT). The incoming laser output is reflected from the first metallic mirror and divided into two parts by the first beam splitter (BS–1). One part of the light is reflected by moving corner cube metallic mirror which is driven by a signal generator and comes to second beam splitter. The other part goes through the first beam splitter and is reflected back from the second corner cube mirror to the second beam splitter (BS–2). On the surface of the second beam splitter, the reflected beams will come together and get focused by a parabolic mirror which has a focal length of 2.5 mm onto the 0.5 mm

long second harmonic generation crystal (SHG x–tal). Length of the SHG crystal was chosen to be short not to encounter any bandwidth limitation. BBO (beta-Barium Borate) crystal was used in the experiments. Depending on the intensity of the interference, the SHG crystal generates second harmonic of the incident light. The generated signal intensity depends on

$$I \sim \left({}^{\omega^4}/_{c^3} \right) (p\Lambda)^2 \left({}^{V}/_{\Lambda} \right) \qquad \text{(A.1)}$$

for the focused beam volume V. Here, ω is the angular frequency of the second harmonic, c velocity of light and Λ is the effective volume of coherence [54].

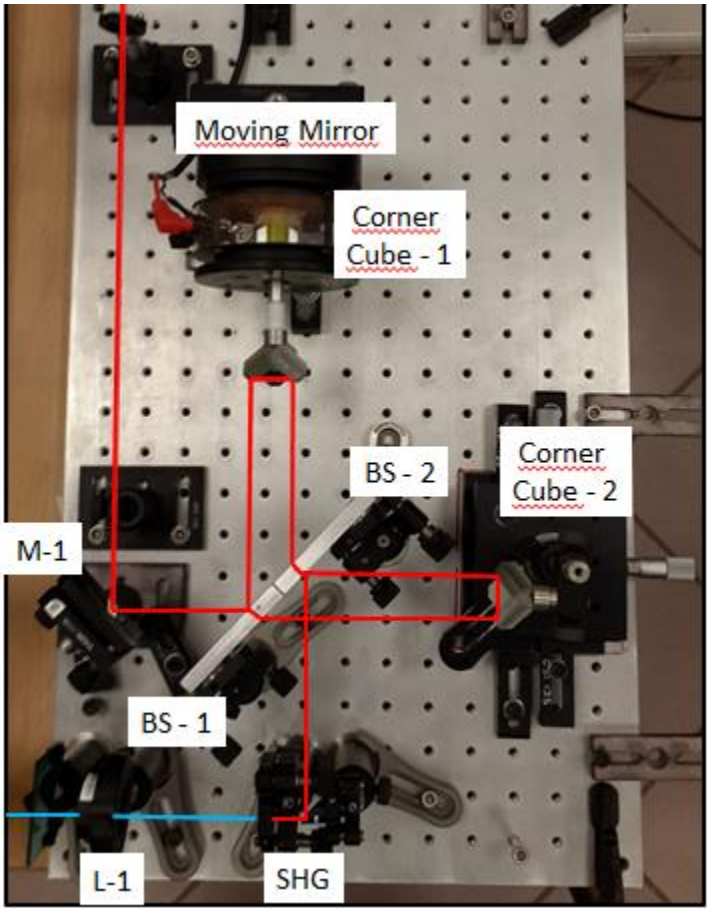

Figure A. 2 : The picture of autocorrelator setup

In the final stage, a photo multiplier tube (PMT) absorbs the second harmonic signal and transfers it to an electric current which is monitored with a digital oscilloscope. Since the PMT used in the experiments was not sensitive to wavelengths above 700 nm, most of the 850-nm light is blocked and we only read the second harmonic signal from the oscilloscope. However, we still used a filter that cuts the wavelengths near the laser output (~850 nm). The obtained signal form can be seen from Fig. A.3.

The autocorrelation trace ratio will be 8–1 as can be seen from Fig. A.3.

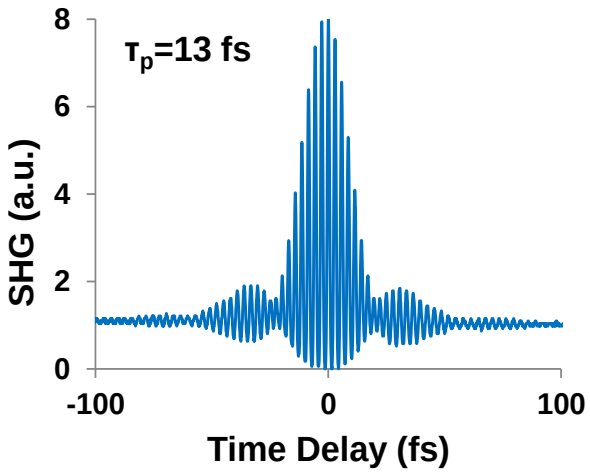

Figure A.3: The interferometric autocorrelation signal

When the ratio is obtained, the time difference between two cycles must be calculated using the relations below:

$$\nu = \frac{c}{\lambda} \tag{A.2}$$

$$T = \frac{1}{\nu} \tag{A.3}$$

$$\tau_p = \frac{T}{\text{autocorrelation factor}} \tag{A.4}$$

Autocorrelation factor is 1.55 for $sech^2$ pulse shape and 1.78 for the pulse spectrum obtained in our experiments with the Cr:LiSAF laser.

APPENDIX B : CAVITY ANALYSIS

To provide a qualitative description about stability range of a laser, stability analysis will be discussed briefly starting with the ray optics picture. At the design step of a laser, resonator stability conditions must be considered to guarantee the confinement of the laser beam. Another important parameter issue is the determination of the laser beam size at any location inside the laser resonator. Simply, using geometric optics and matrix analysis (ABCD matrix) one can determine the conditions for stability. However, it is not that simple to obtain the beam size and radius of curvature at any location only by geometric optics. Therefore, after we discuss ray optics, we will continue with the Gaussian beam analysis and four mirror cavity stability analysis. Additionally, we will analyze our cavity design.

Starting with the ray definition,

$$\vec{U} = \begin{bmatrix} \mathbf{r} \\ \boldsymbol{\theta} \end{bmatrix} \tag{B.1}$$

in ray optics, we can denote $\vec{U}$ as the ray vector which contains the height r from the optic axis and θ which is the angle of inclination of the ray made with the optic axis. Each optical element has aray transformation matrix M_T of the form

$$M_T = \begin{bmatrix} A & B \\ C & D \end{bmatrix}, \tag{B.2}$$

which describes how the ray height and angle will be modified. In a cavity design, consisting of two highly reflecting mirrors, to reach m+1th ray vector $\vec{U}_{m+1}$ information, starting with mth round trip ray vector $\vec{U}_m$ (ray vector after a round trip at the same position), and using transformation matrix, we can obtain the relations below:

$$\vec{U}_{m+1} = M_T \vec{U}_m$$

(B.3.a)

$$r_{m+1} = Ar_m + B\theta_m \tag{B.3.b}$$

$$\theta_{m+1} = Cr_m + D\theta_m \tag{B.3.c}$$

By using Eq. B.3 (b) and Eq. B.3 (c)

$$\theta_m = \frac{r_{m+1} - A r_m}{B} \quad \text{(B.4.a)}$$

$$\theta_{m+1} = \frac{r_{m+2} - A r_{m+1}}{B} \quad \text{(B.4.b)}$$

$$\theta_{m+1} = \frac{D r_{m+1} - (AD - BC) r_m}{B} \quad \text{(B.4.c)}$$

relations can be found. Eliminating θ dependence and using Eqs B.4 (b) and B.4 (c), we obtain

$$r_{m+2} - (A - D) r_{m+1} + (AD - BC) r_m = 0 \quad \text{(B.5)}$$

After a round trip inside the resonator, the ray comes back to its first position and provides the solution (with real φ values)

$$r_m = r_{m0} \exp(i\varphi) \quad \text{(B.6)}$$

Hence,

$$\exp(i\varphi) = \frac{A+D}{2} \pm i\sqrt{1 - \left(\frac{A+D}{2}\right)^2} \quad \text{(B.7)}$$

If φ is real

$$\left|\frac{A+D}{2}\right| \leq 1 \quad \text{(B.8)}$$

condition must be satisfied. When Eq. B.8 is satisfied, this shows us that the height of the ray is bounded and the optical resonator is stable.

ABCD analysis is suitable for Gaussian beam analysis as well. First the complex q–parameter of a Gaussian beam needs to be introduced according to

$$\frac{1}{q(z)} = \frac{1}{R(z)} - i\frac{\lambda}{n_0 \pi \omega^2(z)} \quad \text{(B.9)}$$

The q parameter carries all information for a Gaussian beam such as the radius of curvature (R(z)) and spotsize ($\omega^2(z)$) of the beam at any location along the direction of propagation. To analyze the Gaussian beam inside a paraxial resonator, we need to write down q parameter variation after a round trip

$$q_{n+1} = \frac{A q_n + B}{C q_n + D} \quad \text{(B.10)}$$

Since the beam satisfying the boundary conditions is self–consistent and the analysis does not depend on which roundtrip that we are analyzing, we can write

$$q = \frac{Aq + B}{Cq + D} \quad \text{(B.11)}$$

and using the stability condition $AD - BC = 1$,

$$\frac{1}{q} = \frac{D-A}{2B} \pm i\sqrt{\frac{1-\left(\frac{A-D}{2}\right)^2}{B^2}} \tag{B.12}$$

By using Eq. B.9 and Eq. B.12, the components of the q–parameter can be written in terms of the ABCD matrix elements as

$$\frac{1}{R} = \frac{D-A}{2B} \tag{B.13}$$

$$\frac{\lambda}{n_0 \pi \omega^2(z)} = \frac{\sqrt{1-\left(\frac{A+D}{2}\right)^2}}{|B|} \tag{B.14}$$

Continuing with the four mirror cavity analysis, a standard x–fold cavity design is shown in Fig. B.1.

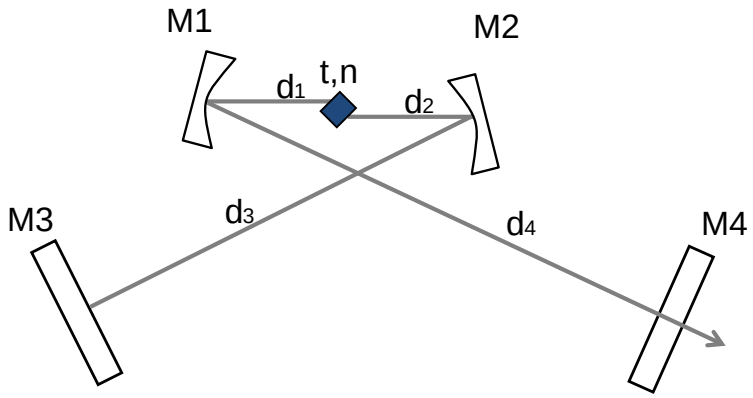

Figure B.1: A schematic of the standard x–fold cavity

The transformation matrix of the given x–fold cavity for a round trip, starting from the plane of M3 mirror is given as

$$M_T = \begin{bmatrix} A & B \\ C & D \end{bmatrix} = \begin{pmatrix} 1 & d_3 \\ 0 & 1 \end{pmatrix} \begin{pmatrix} 1 & 0 \\ -\frac{2}{R_2} & 1 \end{pmatrix} \begin{pmatrix} 1 & d_2 \\ 0 & 1 \end{pmatrix} \begin{pmatrix} 1 & \frac{t}{n} \\ 0 & 1 \end{pmatrix} \begin{pmatrix} 1 & d_1 \\ 0 & 1 \end{pmatrix} \begin{pmatrix} 1 & 0 \\ -\frac{2}{R_1} & 1 \end{pmatrix}$$
$$\begin{pmatrix} 1 & 2d_4 \\ 0 & 1 \end{pmatrix} \begin{pmatrix} 1 & 0 \\ -\frac{2}{R_1} & 1 \end{pmatrix} \begin{pmatrix} 1 & d_1 \\ 0 & 1 \end{pmatrix} \begin{pmatrix} 1 & \frac{t}{n} \\ 0 & 1 \end{pmatrix} \begin{pmatrix} 1 & d_2 \\ 0 & 1 \end{pmatrix} \begin{pmatrix} 1 & 0 \\ -\frac{2}{R_2} & 1 \end{pmatrix} \begin{pmatrix} 1 & d_3 \\ 0 & 1 \end{pmatrix} \quad \text{(B.15)}$$

Here t is the length of the crystal, n is refractive index of it, d_1–d_4 are distance parameters and R_1 and R_2 are the radius of curvature of cavity curved mirrors. The cavity will be stable for the values of $\left|\frac{A+D}{2}\right| \leq 1$ and the Rayleigh range on M3 can be calculated from

$$z_0 = \frac{|B|}{\sqrt{1-\left(\frac{A+D}{2}\right)^2}} \quad \text{(B.16)}$$

To calculate the beam waist inside the crystal using the knowledge of the Rayleigh range on M3, we need to cut the left side of the cavity off which can be seen from Fig. B.2.

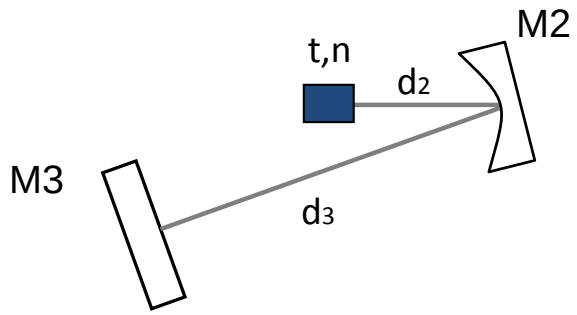

Figure B.2:Part of the cavity used in the calculation of the beam waist inside the crystal

The transformation matrix of the given part of the cavity starting from the focus position on M5 will be

$$M_T = \begin{bmatrix} A' & B' \\ C' & D' \end{bmatrix} = \begin{pmatrix} 1 & d_3 \\ 0 & 1 \end{pmatrix} \begin{pmatrix} 1 & 0 \\ -\frac{2}{R_2} & 1 \end{pmatrix} \begin{pmatrix} 1 & d_2 \\ 0 & 1 \end{pmatrix} \quad \text{(B.17)}$$

The location of the focus and Rayleigh range of the collimated beam inside the crystal can be calculated by using the equations[39]

$$d_f = -n\frac{[D'B'+A'C'z_0^2]}{\left(D'^2+z_0^2C'^2\right)} \tag{B.18}$$

$$z_0' = \frac{nz_0}{\left(D'^2+z_0^2C'^2\right)} \tag{B.19}$$

Using the matrix given in Eq. B.17, we calculated the distance of focus and variation of the beam waist inside the crystal as shown in Fig. B.3 and Fig. B.4

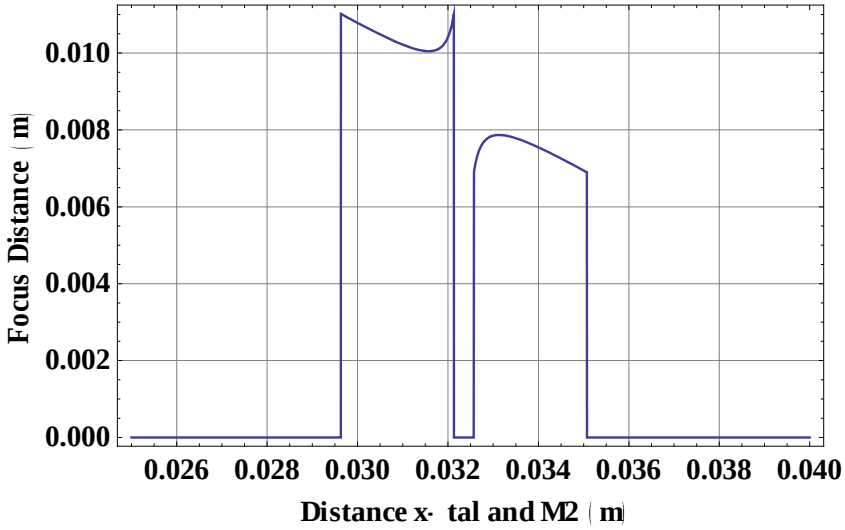

Figure B. 3: Variation of the beam waist position inside the crystal with respect to the distance between the edge of the crystal and the first mirror.

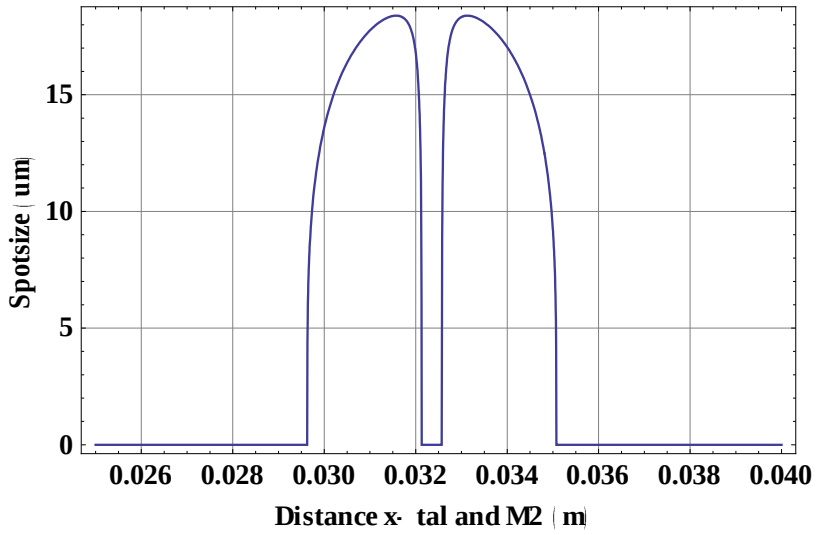

Figure B. 4: Calculated variation of the beam waist inside the gain crystal as a function of the distance between the edge of the crystal and the first mirror.

As mentioned before, using GMOC makes it possible to obtain mode–locked operation via KLM without approaching the edge of the stability range. The calculated stability range of the prismless Cr:LiSAF cavity is shown in Fig. B.3 and B.4. The distance between the Cr:LiSAF crystal and M2 at which KLM operation is obtained is 0.033 m. To ability obtain KLM operation, by the help of the GMOC nearly at the center of the stability range, provides higher beam quality and higher average output power.

VITA

Ferda Canbaz was born in Pehlivanköy, Kırklareli on June 2, 1988. She received her BS degree in Physics engineering from Istanbul Technical University. During her undergraduate study, between 2008 and 2010, she worked as an intern in the Material Preparation and Optical Characterization Laboratory. In 2011, she worked as an intern in Laser Processing Laboratory. In 2011, she was admitted to the Master of Science program in Optoelectronics and Photonics Engineering at Koç University. Her research interests include near–infrared solid state lasers, spectroscopy of doped gain crystals and glasses, and material processing. She will continue her Ph. D. study at Koç University in the same research area.

Publications:

- A. K. Turkoglu, T. Ersoy, F. Canbaz, S. Akturk, "Effects of waveguide behavior during femtosecond–laser drilling of metals", Applied Physics A, Vol. 108, Iss. 4, pp 935–941, (2012)

Proceedings:

- A. K. Turkoglu, F. Canbaz, S. Akturk, "Metallerin femtosaniye lazerlerle işlenmesinde dalgaklavuzu etkileri, Fotonik 2011, 13. Ulusal Optik, Elektro–Optik ve Fotonik Çalıştayı, Bilkent University, İstanbul, Türkiye, (2011)
- Ferda Canbaz, Ersen Beyatlı, Li–Jin Chen, Alphan Sennaroğlu, Franz X. Kaertner, and Ümit Demirbaş, "Cr:LiSAF lazerinden 15–fs altı stabil ve verimli darbe üretimi", Fotonik 2013, 15. Ulusal Optik, Elektro–Optik ve Fotonik Çalıştayı, ASELSAN, Ankara, Türkiye,
- Ferda Canbaz, Ersen Beyatlı, Li–Jin Chen, Alphan Sennaroglu, Franz X. Kaertner, and Umit Demirbas, "Efficient and Robust Kerr –Lens Mode–Locking of Cr:LiSAF Lasers Using Gain–Matched Output Couplers", to be presented at ASSL 2013, Advanced Solid State Lasers Congress, (October 27 – November 2, 2013, Paris, France).

5 REFERENCES

[1] S. K. D. P. P. Pronko, J. Squier, J. V. Rudd, D. Du, G. Mourou, "*Machining of sub-micron holes using a femtosecond laser at 800 nm*," Opt Commun **114**, 106-110 (1995).

[2] D. A. G. Robertson, M. J. P. Dymott, A. I. Ferguson, and G. L. Hogg, "*Two-photon fluorescence microscopy with a diode-pumped Cr:LiSAF laser*," Appl Optics **36**, 2481-2483 (1997).

[3] H. Gebavi, D. Ilanese, R. Balda, S. Chaussedent, M. Ferrari, J. Fernandez, and M. Ferraris, "*Spectroscopy and optical characterization of thulium doped TZN glasses*," Journal of Physics D: Applied Physics **43**, 135104 (2010).

[4] H. Kalaycioglu, H. Cankaya, M. N. Cizmeciyan, A. Sennaroglu, and G. Ozen, "*Spectroscopic investigation of Tm^{3+}: TeO_2-WO_3 glass*," J Lumin **128**, 1501-1506 (2008).

[5] R. H. V. J. Srinivasan, I. Gorczynska, and J. G. Fujimoto, J. Y. Jtang, P. Retsen, and A. E. Cable, "*High-speed, high-resolution optical coherence tomography retinal imaging with a frequency-swept laser at 850 nm*," Opt Lett **32**, 361-363 (2007).

[6] M. D. Young, S. Backus, C. Durfee, and J. Squier, "*Multiphoton imaging with a direct-diode pumped femtosecond Ti:sapphire laser*," J Microsc-Oxford **249**, 83-86 (2013).

[7] R. Ell, U. Morgner, F. X. Kartner, J. G. Fujimoto, E. P. Ippen, V. Scheuer, G. Angelow, T. Tschudi, M. J. Lederer, A. Boiko, and B. Luther-Davies, "*Generation of 5-fs pulses and octave-spanning spectra directly from a Ti:sapphire laser*," Opt Lett **26**, 373-375 (2001).

[8] P. F. Moulton, "*Spectroscopic and laser characteristics of Ti-Al_2O_3*," J Opt Soc Am B **3**, 125-133 (1986).

[9] J. Harrison, A. Finch, D. M. Rines, G. A. Rines, and P. F. Moulton, "L*ow-threshold, cw, all-solid-state Ti-Al_2O_3 laser*," Opt Lett **16**, 581-583 (1991).

[10] P. W. Roth, A. J. Maclean, D. Burns, and A. J. Kemp, "*Directly diode-laser-pumped Ti:sapphire laser*," Opt Lett **34**, 3334-3336 (2009).

[11] D. E. Spence, Kean, P. N., Sibbett, W., "*60-fsec pulse generation from a self-mode-locked Ti:sapphire laser*," Opt Lett **16** (1991).

[12] U. Demirbas, D. Li, J. R. Birge, A. Sennaroglu, G. S. Petrich, L. A. Kolodziejski, F. X. Kartner, and J. G. Fujimoto, "*Low-cost, single-mode diode-pumped Cr:Colquiriite lasers*," Opt Express **17**, 14374-14388 (2009).

[13] S. A. Payne, L. L. Chase, H. W. Newkirk, L. K. Smith, and W. F. Krupke, "*$LiCaAlF_6:Cr^{3+}$: A promising new solid-state laser material*," Ieee J Quantum Elect **24**, 2243-2252 (1988).

[14] S. A. Payne, L. L. Chase, L. K. Smith, W. L. Kway, and H. W. Newkirk, "*Laser performance of $LiSAIF_6:Cr^{3+}$*," Journal of Applied Physics **66**, 1051-1056 (1989).

[15] L. K. Smith, S. A. Payne, W. L. Kway, L. L. Chase, and B. H. T. Chai, "*investigation of the laser properties of Cr^{3+}:$LiSrGAF_6$*," Ieee J Quantum Elect **28**, 2612-2618 (1992).

[16] E. Sorokin, "*Solid-state materials for few-cycle pulse generation and amplification*," in *Top Appl Phys*, vol. 95, *Topics in Applied Physics*, F. X. Kartner, Ed. (Springer-Verlag, 2004) pp. 3-71.

[17] F. Druon, F. Balembois, and P. Georges, "*New laser crystals for the generation of ultrashort pulses*," Cr Phys **8**, 153-164 (2007).

[18] L. J. Atherton, S. A. Payne, and C. D. Brandle, "*Oxide and fluoride laser crystals*," Annu Rev Mater Sci **23**, 453-502 (1993).

[19] L. H. Wei, P. K. Kuo, R. L. Thomas, T. R. Anthony, and W. F. Banholzer, "T*hermal-conductivity of isotopically modified single-crystal diamond*," Phys Rev Lett **70**, 3764-3767 (1993).

[20] S. Uemura and K. Torizuka, "*Generation of 10 fs pulses from a diode-pumped Kerr-lens mode-locked Cr:LiSAF laser*," Jpn J Appl Phys 1 **39**, 3472-3473 (2000).

[21] P. C. Wagenblast, U. Morgner, F. Grawert, T. R. Schibli, F. X. Kartner, V. Scheuer, G. Angelow, and M. J. Lederer, "*Generation of sub-10-fs pulses from a Kerr-lens mode-locked Cr^{3+}:LiCAF laser oscillator by use of third-order dispersion-compensating double-chirped mirrors*," Opt Lett **27**, 1726-1728 (2002).

[22] I. T. Sorokina, E. Sorokin, E. Wintner, A. Cassanho, H. P. Jenssen, and M. A. Noginov, "*Efficient continuous-wave $TEM_{(00)}$ and femtosecond Kerr-lens mode-locked Cr:LiSrGaF laser*," Opt Lett **21**, 204-206 (1996).

[23] C. G. Leburn, W. Lu, S. Vetter, M. D. Dawson, C. T. A. Brown, J. S. Harris, S. Calvez, and W. Sibbett, "*650MHz-prf-femtosecond $Cr^{(4+)}$:forsterite laser with*

dispersion-compensating GaInNAs SESAM," 2011 Conference on Lasers and Electro-Optics (Cleo) (2011).

[24] C. G. Leburn, N. K. Metzger, C. T. A. Brown, W. Sibbett, S. Calvez, D. Burns, H. D. Sun, M. D. Dawson, M. Le Du, and J. C. Harmand, "*Femtosecond pulse generation at 1530 nm using a GaInNAsSb SESAM*," 2008 Conference on Lasers and Electro-Optics & Quantum Electronics and Laser Science Conference, Vols 1-9, 198-199 (2008).

[25] B. E. Bouma, G. J. Tearney, I. P. Bilinsky, B. Golubovic, and J. G. Fujimoto, "*Self-phase-modulated Kerr-lens mode-locked Cr:forsterite laser source for optical coherence tomography*," Opt Lett **21**, 1839-1841 (1996).

[26] M. N. Cizmeciyan, H. Cankaya, A. Kurt, and A. Sennaroglu, "*Operation of femtosecond Kerr-lens mode-locked Cr:ZnSe lasers with different dispersion compensation methods*," Appl Phys B-Lasers O **106**, 887-892 (2012).

[27] S. Spalter, M. Bohm, M. Burk, B. Mikulla, R. Fluck, I. D. Jung, G. Zhang, U. Keller, A. Sizmann, and G. Leuchs, "*Self-starting soliton-modelocked femtosecond $Cr^{(4+)}$:YAG laser using an antiresonant Fabry-Perot saturable absorber*," Appl Phys B-Lasers O **65**, 335-338 (1997).

[28] K. M. Gabel, P. Russbuldt, R. Lebert, and A. Valster, "*Diode pumped Cr^{3+}: LiCAF fs-laser*," Opt Commun **157**, 327-334 (1998).

[29] V. P. Yanovsky, F. W. Wise, A. Cassanho, and H. P. Jenssen, "*Kerr-Lens mode-locked diode-pumped Cr-Lisgaf laser*," Opt Lett **20**, 1304-1306 (1995).

[30] J. R. Lincoln, M. J. P. Dymott, and A. I. Ferguson, "*Femtosecond pulses from an all-solid-state Kerr-Lens mode-locked Cr:LiSAF laser*," Opt Lett **19**, 1210-1212 (1994).

[31] R. Scheps, J. F. Myers, H. B. Serreze, A. Rosenberg, R. C. Morris, and M. Long, "*Diode-pumped Cr-LiSrAlF_6 laser*," Opt Lett **16**, 820-822 (1991).

[32] G. J. Valentine, J. M. Hopkins, P. LozaAlvarez, G. T. Kennedy, W. Sibbett, D. Burns, and A. Valster, "*Ultralow-pump-threshold, femtosecond Cr^{3+}:LiSrAlF_6 laser pumped by a single narrow-stripe AlGaInP laser diode*," Opt Lett **22**, 1639-1641 (1997).

[33] S. Tsuda, W. H. Knox, and S. T. Cundiff, "*High efficiency diode pumping of a saturable Bragg reflector-mode-locked Cr:LiSAF femtosecond laser*," Appl Phys Lett **69**, 1538-1540 (1996).

[34] G. J. Valentine, J. M. Hopkins, P. LozaAlvarez, G. T. Kennedy, W. Sibbett, D. Burns, and A. Valster, "*Ultralow-pump-threshold, femtosecond Cr^{3+}:LiSrAlF_6 laser pumped by a single narrow-stripe AlGaInP laser diode*," Opt Lett **22**, 1639-1641 (1997).

[35] A. A. Lagatsky, C. T. A. Brown, and W. Sibbett, "*Highly efficient and low threshold diode-pumped Kerr-lens mode-locked Yb : KYW laser*," Opt Express **12**, 3928-3933 (2004).

[36] W. Sibbett, A. A. Lagatsky, and C. T. A. Brown, "*The development and application of femtosecond laser systems*," Opt Express **20**, 6989-7001 (2012).

[37] L. J. Chen, M. Y. Sander, and F. X. Kartner, "*Kerr-lens mode locking with minimum nonlinearity using gain-matched output couplers*," Opt Lett **35**, 2916-2918 (2010).

[38] L. J. Chen, M. Y. Sander, and F. X. Kartner, "*Mode Locking with Minimum Nonlinearity Using Inverse-Gain Output Couplers*," 2010 Conference on Lasers and Electro-Optics (Cleo) and Quantum Electronics and Laser Science Conference (Qels) (2010).

[39] A. Sennaroglu, *Photonics and laser engineering : principles, devices, and applications* (McGraw-Hill, 2010).

[40] A. Einstein, "*On the quantum theory of radiation*," Physikalische Zeitschrift **18**, 121-128 (1917).

[41] B. C. Young, F. C. Cruz, W. M. Itano, and J. C. Bergquist, "*Visible lasers with subhertz linewidths*," Phys Rev Lett **82**, 3799-3802 (1999).

[42] H. Abramczyk, *Introduction to Laser Spectroscopy*, 1st edition ed (Elsevier, 2005).

[43] Y. P. Tong, J. M. Sutherland, P. M. W. French, J. R. Taylor, A. V. Shestakov, and B. H. T. Chai, "*Self-starting Kerr-lens mode-locked femtosecond Cr^{4+}:YAG and picosecond Pr^{3+}:YLF solid-state lasers*," Opt Lett **21** (1996).

[44] I. T. Sorokina, E. Sorokin, E. Wintner, A. Cassanho, H. P. Jenssen, and R. Szipocs, "*14-fs pulse generation in Kerr-lens mode-locked prismless Cr:LiSGaF and Cr:LiSAF lasers: observation of pulse self-frequency shift*," Opt Lett **22**, 1716-1718 (1997).

[45] S. H. Cho, Bouma, B.E., Ippen, E.P., Fujimoto, J.G., "*Low-repetition-rate high-peak-power Kerr-lens mode-locked Ti:Al_2O_3 laser with a multiple-pass cavity*," Opt Lett **24**, 417-419 (1999).

[46] M. N. Cizmeciyan, H. Cankaya, A. Kurt, and A. Sennaroglu, "*Kerr-lens mode-locked femtosecond Cr^{2+}:ZnSe laser at 2420 nm*," Opt Lett **34**, 3056-3058 (2009).

[47] F. X. Kaertner, "*Ultrafast optics, Kerr-Lens and Additive Pulse Mode Locking*." http://ocw.mit.edu/courses/electrical-engineering-and-computer-science/6-977-ultrafast-optics-spring-2005/lecture-notes/chapter7.pdf, 2005, pp. 258.

[48] H. A. Haus, "*Mode-locking of lasers*," Ieee J Sel Top Quant **6**, 1173-1185 (2000).

[49] E. B. Treacy, "*Optical Pulse Compression with Diffraction Gratings*," Ieee J Quantum Elect **5**, 454-458 (1969).

[50] R. L. Fork, C. H. B. Cruz, P. C. Becker, and C. V. Shank, "*Compression of optical pulses to six femtoseconds by using cubic phase compensation*," Opt Lett **12**, 483-485 (1987).

[51] S. A. Payne, W. F. Krupke, L. K. Smith, W. L. Kway, L. D. Deloach, and J. B. Tassano, "*752 nm wing-pumped Cr-Lisaf laser*," Ieee J Quantum Elect **28**, 1188-1196 (1992).

[52] F. X. Kartner, N. Matuschek, T. Schibli, U. Keller, H. A. Haus, C. Heine, R. Morf, V. Scheuer, M. Tilsch, and T. Tschudi, "*Design and fabrication of double-chirped mirrors*," Opt Lett **22**, 831-833 (1997).

[53] S. Uemeura and K. Torizuka, "*Generation of 12-fs pulses from a diode-pumped Kerr-lens mode-locked Cr:LiSAF laser*," Opt. Lett. **24**, 780-782 (1999).

[54] A. E. H. P. A. Franken, C. W. Peters, and G. Weinreich, "G*eneration of optical harmonics*," Phys Rev Lett **7**, 118-119 (1961).